Folded Lightweight Actuated Position System (FLAPS) for CubeSat Deployables

by

Paula do Vale Pereira

B.S. in Mechanical Eng., Federal University of Santa Catarina, 2014
B.B.A. in Business Admin., State University of Santa Catarina, 2015
S.M. in Mechanical Eng., Federal University of Santa Catarina, 2017

Submitted to the Department of Aeronautics and Astronautics
in partial fulfillment of the requirements for the degree of

Master of Science in Aeronautics and Astronautics

at the

MASSACHUSETTS INSTITUTE OF TECHNOLOGY

June 2019

Author ..... Signature redacted .....
Department of Aeronautics and Astronautics
May 23, 2019

Certified by ..... Signature redacted .....
Kerri Cahoy
Associate Professor of Aeronautics and Astronautics
Thesis Supervisor

Accepted by ..... Signature redacted .....
Sertac Karaman
Associate Professor of Aeronautics and Astronautics
Chair, Graduate Program Committee

Folded Lightweight Actuated Position System (FLAPS) for CubeSat Deployables

by

Paula do Vale Pereira

Submitted to the Department of Aeronautics and Astronautics
on May 23, 2019, in partial fulfillment of the
requirements for the degree of
Master of Science in Aeronautics and Astronautics

Abstract

Precision actuation of mechanical structures on small spacecraft is challenging. Currently the solutions include single-use actuators based mainly on pyrotechnics and springs, and multiple-use actuators that typically consume more size, weight, and power than available on CubeSats. Multiple-use actuators may also be complex with several moving parts and a higher probability of failure. The Folded Lightweight Actuated Positioning System (FLAPS) demonstrates the use of shape memory alloy (SMA) strips along with a feedback control loop as a repeatable use actuator for small satellites. SMAs are metal alloys that remember a stored shape when transitioning to the austenitic phase at a certain temperature, and are easily deformable in the martensitic phase. The transition temperature is well-defined and typically ranges from 0°C to 90°C. The SMA used in this work was nitinol and had a transition temperature of 80°C. To program the shape, the SMA was trained by high-temperature annealing, being placed in a mold in an oven at 500°C for approximately 30 minutes. The FLAPS mechanism consists of a pair of SMA strips that actuate in opposition and are mounted to a hinge assembly; one side of the hinge is attached to the satellite bus model and the other side of the hinge is attached to a solar panel model. We use a magnetic encoder to provide feedback to the developed controller board and algorithms, actuating the SMA hinge. Current is applied to the SMA strip and Joule heating actuates the SMA, consuming at most 1 W of power. The current FLAPS prototype has shown to be small, lightweight (35 g), repeatable and precise (error within 2°). The range of actuation of the hinge is yet to be increased, being currently only 18°. The FLAPS team will validate the actuator system and collect angle responses in a microgravity environment on a parabolic flight in the summer of 2019.

Thesis Supervisor: Kerri Cahoy
Title: Associate Professor of Aeronautics and Astronautics

Acknowledgments

I would like to thank everyone that somehow has helped me in the development of not only this thesis, but myself as a whole during the last couple of years. Firstly, I would like to thank Professor Kerri Cahoy for accepting me in her lab last Spring, for allowing me to pursue my research interests, and, more than anything, for supporting me to pursue my life goals and advocating for me no matter what.

I would also like to thank the FLAPS team for their hard work and for the many bittersweet nights in the lab, when we would be mostly disappointed by the results, but happy for the joyful company: Katie Chun, Mario Contreras, Charles Lindsay, Shreeyam Kacker, and Raymond Huffman. I also can't forget Christian Haughwout, who developed the first FLAPS prototype a couple of years ago and served as a mentor for our team throughout the last year.

I would also like to thank the STAR Lab team, which helped with suggestions on the project and by simply being the great friends they are. I'd like to send special acknowledgements to my office mates Rachel Morgan, Maddy Lambert, and Yinzi Xin, and to the members of the teams of the other projects I'm part of and that understood when FLAPS needed my attention: DeMi team, MOSAIC team, CLICK team, and C3 team.

I would like to thank the friends that are not from the lab, but that have made an enormous impact in my work and my mental health: GWAE Outreach Team (Regina, Golda, Soumya, and Rachel), REFS Team (Regina, Golda, Aaron, Christine, Mohammad, Maya, and Heng), my friends from Brazil (Rorato, George, Douglas, Lucao), the qualifying exam study group, my fellow AeroAstro Brazilian student Diogo Castilho, my math Professor who ended up becoming a great friend (and proofreader of this thesis) Matthew Durey, and, of course, my boyfriend Felipe Depine.

Lartly, I would like to send warm thoughts to Brazil, where my entire family is and where I was born and raise. Nothing would have been possible without my mother Kari Avila do Vale Pereira, my father Dylton do Vale Pereira Filho, my sister Rafaela do Vale Pereira, and my brother in law Claudio Jose Santos. Last month, my father

suffered a severe accident and was almost 30 days in the intensive care unit in the hospital, fighting for his life. He is currently recovering at home and is showing great progress due to the gigantic efforts of my mother and my sister – who have completely paused their lives to focus on taking care of my father and allowing me to continue pursing my studies in the USA.

THANK YOU SO MUCH!

Contents

List of Figures

List of Tables

Chapter 1

Introduction

There are many different shapes and sizes of satellites orbiting the Earth and the Sun. The famous Hubble Space Telescope is the size of a school bus: 13.2 m long, 4.2 m wide, and 2.4 m diameter aperture. Big satellites are capable of hosting large payloads, are stable in their orbit, and tend to have a longer lifetime in space, but they are also very expensive and take many years to be designed and built.

The current tendency in space is to move towards smaller satellites, which are significantly cheaper than their larger companions and can be designed and built in a much shorter time span. One example is the difference in cost between the 2180 kg Mars Reconnaissance Orbiter (MRO) and the 13.5 kg Mars Cube One (MarCO): while the former costed 720 million dollars [18], the latter costed 18.5 million dollars [5], both can be seen in Fig. 1-1. The performed missions are obviously different, but the lower cost allows the satellites to serve as demonstration platforms for new technologies, increasing the Technology Readiness Level (TRL) of satellite components before implementing them in big satellites, which can substantially decrease the risk of larger missions. Cheaper satellites also allow more people, organizations, and countries to access space, democratizing such important technologies.

The type of small satellite that is succeeding the most in cost minimization is the CubeSat. They are shoe box-sized satellites that follow clear standards and try to use as many commercial off-the-shelf (COTS) devices as possible. The base structure is a 10 cm x 10 cm x 10 cm cube, named "one unit" or "1U" for short. The units can

(a) Mars Reconnaissance Orbiter [18] (b) Mars Cube One [5]

Figure 1-1: Different sizes of satellites.

be combined together to form slightly bigger satellites, like 3U or 6U CubeSats. The inner section of these satellites perfectly fit a PC-104 board, facilitating integration with COTS electronics. The structure is made of aluminum and has three main parts: the rails, which structurally support the components and devices; the walls, which protect the inner components; and the top and bottom caps, which can either support or protect the satellite components.

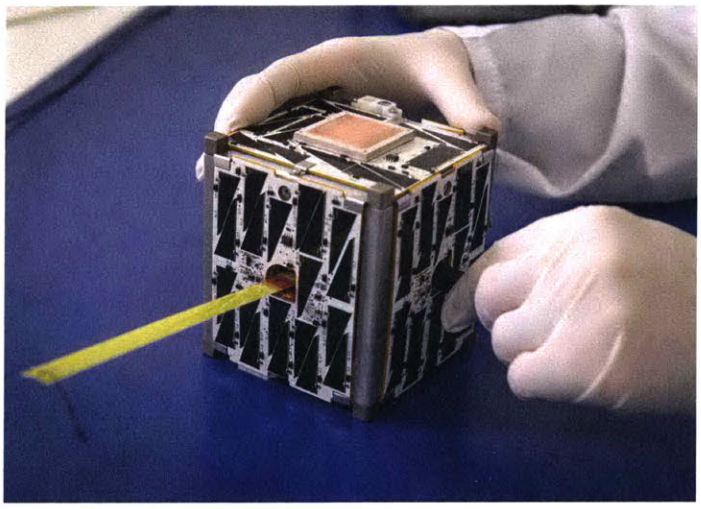

Figure 1-2: An example of a 3U CubeSat from NASA Goddard, 2019 [20]

Small satellites have their own challenges, mainly due to their limited weight, size, and power capacity. New technologies need to be developed to be able to accomplish significant tasks with so little space and power availability. This thesis focuses on one

of these needs: repeatable actuation.

1.1 Actuators in Space

Peter Fortescue in his book Spacecraft Systems Engineering [6] dedicates an entire chapter to spacecraft mechanisms. The largest subsection of the chapter describes single use devices, which are described as a restraining fixture that is destroyed to allow actuation (generally by pyrotechnic devices) and an actuator to enforce a predetermined movement (generally through stored potential energy, like springs). The author discusses features on spring-loaded separation systems, spring-loaded hinges, tape springs, tubular booms, articulated trusses, and inflatable structures. Most of these single use mechanisms can be miniaturized to be used in small satellites.

The author also discusses continuous and intermittent operating devices [6], focusing on attitude control devices, solar array drives, antenna pointing mechanisms, and retractable appendages. The solar array drives are generally composed of shafts, bearings, diaphragms, flanges, motors, and other devices, resulting in large and heavy actuators. The antenna pointing mechanisms involve motors, gearboxes, joints, ring gears, and many other movable components, making them large and heavy actuators as well. The attitude control devices and the retractable appendages are usually made out of heavy moving components, like motors, gears, and momentum wheels.

The actuators used in satellites can be then divided in two main groups: single use actuators and repeatable actuators. To extend on what was found in Fortescue [6], the next sections will cover some characteristics of actuators that have flown in space before.

1.1.1 Single use actuators

Single use actuators tend to be compact and reliable, but are not capable of retracting and adjusting position after deployment.

One common way of actuating solar arrays and other single use mechanisms in rovers and satellites is pyrotechnic [14]. The core of this technique is a device that

holds under tension the item to be deployed, and releases it when the holding mechanism is broken by the explosion of the pyrotechnic element. This type of mechanism is simple, reliable, compact, and gives a fast response, but it can only be used once.

Another common option for single use deployables is the called Frangibolt, from TiNi Aerospace [1]. The mechanism is composed mainly by a bolt with a circular indentation and an external shape memory alloy (SMA) cylinder. When the SMA is activated, it elongates and stretches the bolt, which results in fractures at the indentation when the force limit is reached. Fig. 1-3 shows an overview of how the mechanism parts. The mechanism is simple, reliable, and efficient, but is limited to single use actuation.

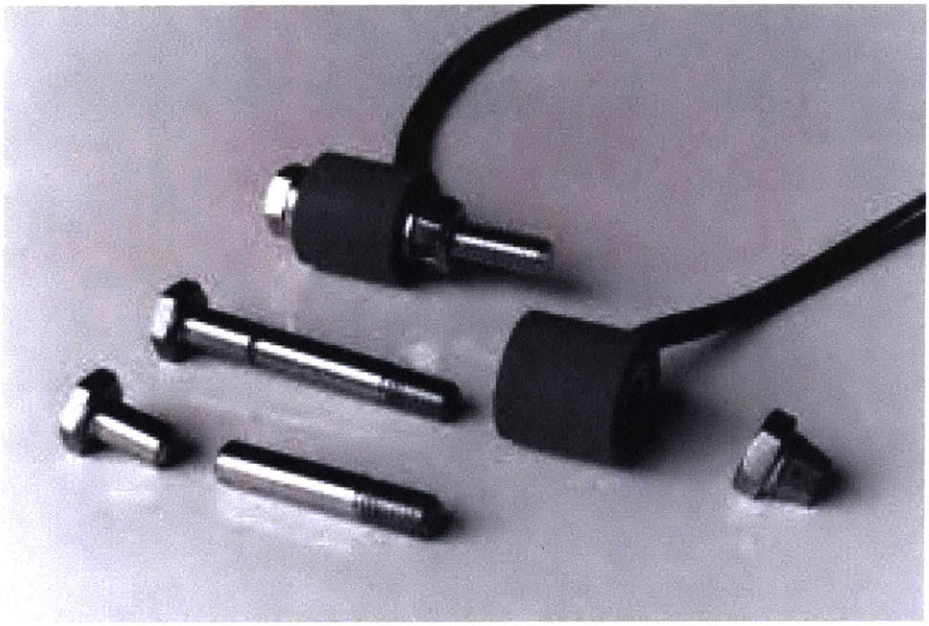

Figure 1-3: The components of the Frangibolt before and after fractures.[1]

The company Sierra Nevada Corporation [3] offers a product called K-truss Boom, which is a single use elastic deployable boom. The spring joints utilize stowed energy for deployment, eliminating the need for a drive motor and electronics, and providing a simple, nonrotating deployment. The company claims that the mechanism is precise, stable, stiff, and mass optimized, and is typically used for solar array, antenna, instrument, and thruster deployments.

1.1.2 Repeatable actuators

Repeatable actuators are used in satellites when the retrieval of the actuated element is desired or necessary. One example is pointing an antenna in the direction of the ground station to optimize the transmission, or moving the solar arrays so that they are facing the sun. The actuators that are generally used in these tasks range from servos to pneumatic actuators.

In 2012 NASA's Jet Propulsion Laboratory launched the NuSTAR Mission [17]. The satellite had a 10 meter long mast designed to detect X-ray signals from objects in the center of the Milky Way, uncovering details of explosion dynamics and nucleosynthesis in supernovae – results that help scientists understand the evolution of massive black holes. The articulated mast was launched stowed inside a one meter canister to allow the satellite to fit in a low cost rocket. The mast was then unfolded, driven by a motor that took around half an hour to complete the task [17]. After deployemeny, the mast length and position can be slightly adjusted to precisely align the optical instruments.

The company Sierra Nevada Corporation [3] also offers a product called Jackscrew Deployed Boom, which is a motor deployed, high stiffness, articulated truss. The mechanism is purely linear and does not require a canister. The attached brushless electric motor allows the boom to be re-stowed after deployment, driving a series of jackscrews that bring the boom back into four structural tubes. The company claims that the mechanism is reliable, stable, stiff, and provides high deployment and retraction forces, and is typically used for solar array, antenna, radar, and instrument deployment and retraction.

Northrop Grumman [7] offers at least six different types of repeatable actuators for space applications: a deployable mesh reflector, a deployable monopole antenna, a telescopic tube mast, a storable tubular extendable member, hinges, and an extendable support structure. Some mechanisms are actuated by motors and others are actuated by the elastic stored energy, but do not have retraction capabilities. According to the company, all the mechanisms have flight heritage and have presented

100% success rates to date. The Storable Tubular Extendable Members are the most compact option and come in many different shapes, as can be seen in Fig. 1-4. They have internal motors that allow deployment and retraction of the tubular member.

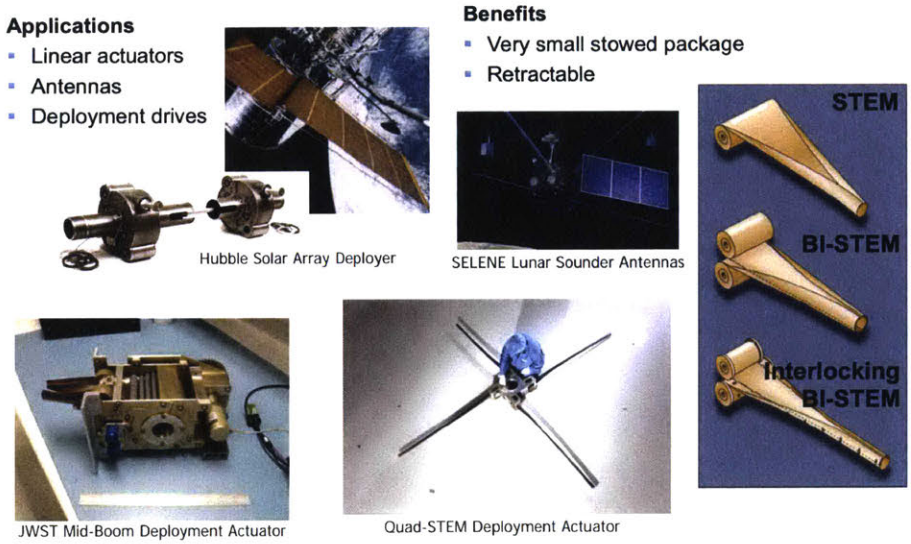

Figure 1-4: Examples of the Storable Tubular Extendable Member from Northrop Grumman. [7]

1.2 Actuators in Small Satellites

The repeatable actuators discussed above require more volume, mass, and power than what a small CubeSat can afford. Hense, the mechanical actuators that have already been developed and used in CubeSats are mostly single use.

Guzik and Benafan [8] worked on the design and development of a deployment mechanism that uses shape memory alloys (SMA). The mechanism deploys the body-mounted solar arrays on each side of a 3U CubeSat. Although the mechanism is planned for a single use in space, the actuator is an SMA strip to allow test and reset on ground prior to launch, reducing the risk of deployment failure. The actuator is comprised of a retention and release (R&R) mechanism and a hinge, both SMA-driven, as can be seen in Fig. 1-5.

The R&R is driven by a linear SMA actuator that releases four springs when activated. The springs then push the release plate, which has two hooks that hold

the solar array in place and are released when the plate is pushed. The hinge is made of aluminum and has a superelastic strip of SMA over it. The SMA applies a constant pushing force on the hinge, actuating it open when the solar panel is released by the R&R mechanism. The authors faced some issues in the assembly due to overstraining and the poor soldering characteristics of the SMA. After testing and iterating the design, the mechanism proved to be effective as a single use actuator for solar array deployment.

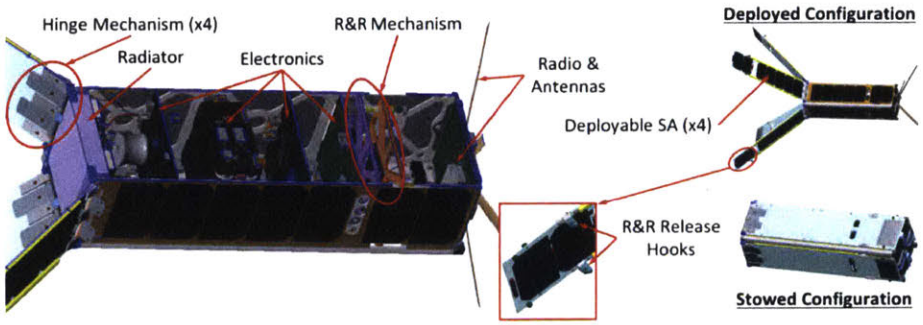

Figure 1-5: Solar array deployment mechanism developed by Guzik and Benafan. [8]

A CubeSat called QuakeSat was developed in a collaboration between the Space Systems Development Laboratory at Stanford University and the R&D division of Stellar Solutions, a company in Palo Alto, CA [15]. The satellite was a proof of concept for detecting earthquakes from space using ultra low frequency radio signals. The antenna boom for that detection had to be 0.701 m long, which is more than double the length of the 3U CubeSat bus that was used. The antenna was a spring-loaded telescopic boom composed of three segments of decreasing diameter aluminum rods. The boom was a single use deployment: it was held in place by the P-Pod launch structure and would deploy as soon as the satellite left the pod. The CubeSat also had deployable solar panels, which were also held in place by the P-Pod structure and would deploy as soon as the satellite was launched. Both single use deployables can be seen in Fig. 1-6.

The company Oxford Space Systems offers an array of deployables for satellites [21]. One deployable, the Astrotube™ Boom, was successfully validated in November 2016 inside a 3U CubeSat called AlSat-Nano. The boom reaches up to two meters

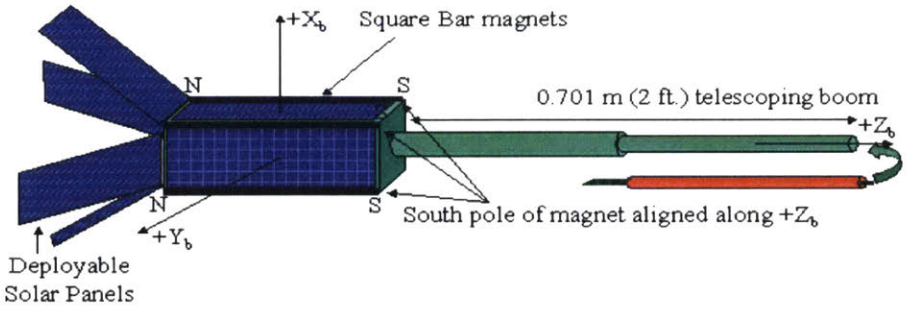

Figure 1-6: Antenna boom and solar panels deployables by Long M. *et al.* [15]

of length and is structured as a tape spring that is actuated by a motor, as can be seen in Fig. 1-7. The presence of a motor allows the boom to be retracted back to its stowed position. The disadvantage of this actuator is its size: it consumes almost one entire unit of a CubeSat.

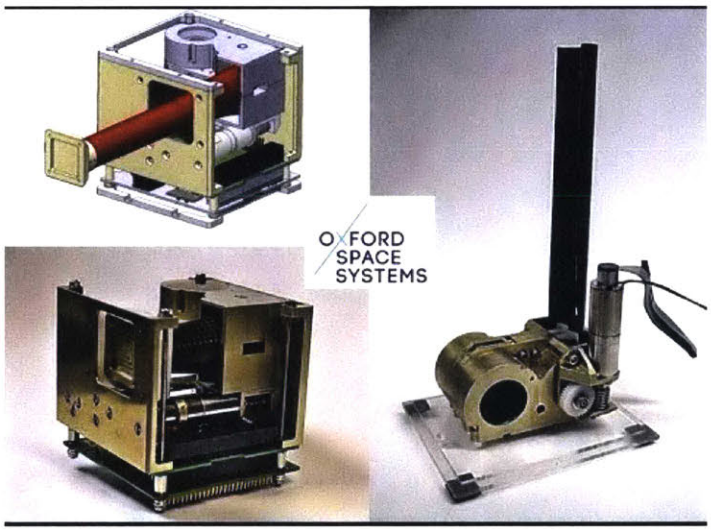

Figure 1-7: Deployable tape spring boom by Oxford Space Systems. [21]

1.3 Technical Gap Addressed

Table 1.1 summarizes the actuators that were described in Sections 1.1 and 1.2 and classifies them as having or not having the characteristics that we are focusing on in this work: repeatable, small, lightweight, and precise. The first column refers to either the name of the technique or the author of the referenced work.

Described Actuators				
Technique or Author	Repeatable	Small	Lightweight	Precise
Pyrotechnic [14]	No	Yes	Yes	No
Frangibolt [1]	No	Yes	Yes	No
K-truss Boom [3]	No	No	Yes	Yes
NuSTAR articulated mast [17]	Yes	No	No	Yes
Jackscrew Deployed Boom [3]	Yes	No	No	Yes
Deployable Mesh Reflector [7]	No	No	No	Yes
Deployable Monopole Antenna [7]	No	Yes	Yes	No
Telescopic Tube Mast [7]	No	No	No	Yes
Storable Tubular Extendable Member [7]	Yes	No	No	Yes
Hinge [7]	Yes	No	No	Yes
Extendable Support Structure [7]	No	No	No	Yes
SMA R&R and hinge [8]	No	Yes	Yes	No
QuakeSat Boom [15]	No	No	Yes	Yes
Astrotube™ Boom [21]	Yes	No	No	Yes

Table 1.1: Characteristics of typical spacecraft actuators

Based on the literature review summarized in Table 1.1, the technical gap is clear: there is currently no actuator that is small, lightweight, and, at the same time, repeatable and precise. This type of actuator is a need in small satellites, which are currently left either with single use actuators or having to allocate a significant part of its volume and mass budgets to a repeatable actuator.

This work addresses the technical gap through the development of a simple, small,

lightweight hinge that provides repeatable and precise actuation to small satellites – a project entitled Folded Lightweight Actuation Precision System (FLAPS).

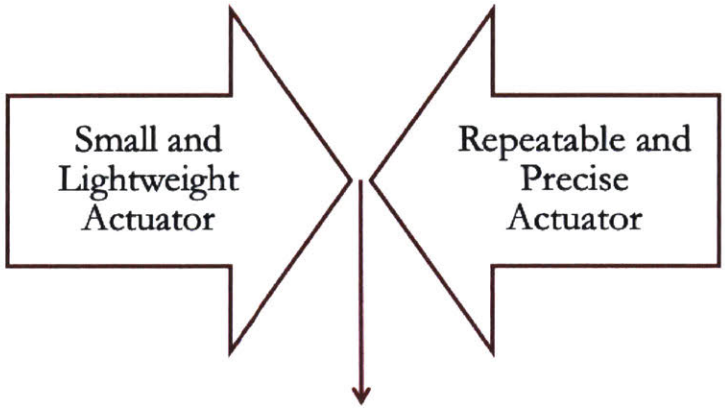

Figure 1-8: Graphical depiction of the technical gap this work intend to close.

1.4 Preview of Following Chapters

Chapter 1 describes the state-of-the-art actuation techniques and the technical gap that this work aims to close. Chapter 2 describes the approach and the main technique that is going to be used to close the technical gap. Chapter 3 describes the prototypes that are developed. Chapter 4 describes the results that have already been achieved, and the future results that are expected to be achieved soon. Finally, Chapter 5 will describe the conclusions of this work and will present the gaps that should be addressed by future research.

Chapter 2

Approach

Actuators need to perform two main tasks: release mechanical energy during deployment and maintain the desired stowed and deployed positions. There are many ways of storing and releasing energy. The most common for repeatable actuators is to use electricity to move motors that will release or retract a mechanism. Single use actuators tend to apply stored potential energy or chemical energy to deploy the mechanism. One special way of storing and releasing energy is used on Frangibolts [1]: they use shape memory alloys (SMA) to break the bolt. This type of material stores energy inside its crystal structure. SMAs can be actuated in many directions and in many shapes, not only for stretching. The second main task of an actuator, to maintain the desired stowed and deployed positions, can be reached through the design of the hinge itself, as will be explained in Chapter 3.

We believe that SMAs have the potential to provide the bending energy necessary to repeatedly actuate a hinge, resulting in a simple, small, lightweight, repeatable, and precise actuator. The following sections will describe how SMAs work and how they are currently being used, serving as a base for our prototype design that will be covered in Chapter 3.

2.1 Shape Memory Alloys

According to the book Shape Memory Alloy Engineering by Lecce and Concilio [13], "shape memory is a specific property some materials have to restore their original shape after a thermal load is applied". When the temperature of a material with shape memory is raised, its residual strains are recovered, creating a macroscopic movement that can be perceived as a cancellation of the applied deformation.

According to the same authors, the shape memory effect is a result of a phase shift, which causes the crystal structure to reorganize. At low temperatures, the stable structure is the martensite, characterized by an eccentric crystal. At high temperatures, the stable structure is the austenite, characterized by a centered cubic structure. A diagram of both phases can be seen in Fig. 2-1. The average temperature in which the structure changes from martensite to austenite is called the transition temperature.

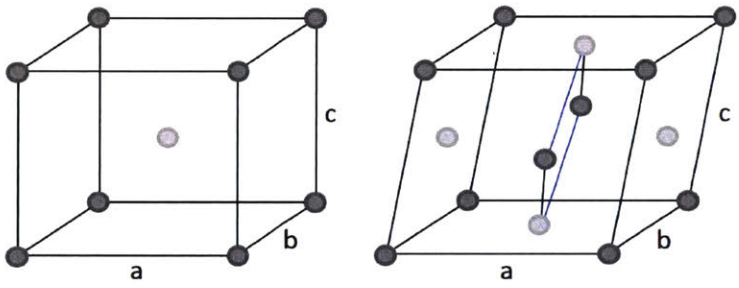

Figure 2-1: Diagrams of an austenite (left) and a martensite (right) geometries. The light gray circles represent atoms of titanium and the dark gray circles represent atoms of nickel. [13]

The transformation between the crystal structures requires small movements of the atoms within the lattice. This occurs over a range of temperatures which are different for each shape memory alloy. [13] The phase transition occurs when the Gibbs free energy of the final phase is less than the Gibbs free energy of the initial phase minus an activation energy. The transformation shows a temperature hysteresis, being characterized by four temperatures:

- M_s: temperature at which the transformation into martensite starts;

- M_f: temperature at which the transformation into martensite finishes;
- A_s: temperature at which the transformation into austensite starts;
- A_f: temperature at which the transformation into austensite finishes.

The transformation into martensite happens during cooling and the transformation into austenite happens during heating. The hysteresis of the transformation varies with the alloy, but generally ranges between 10 and 50°C. Fig. 2-2 shows the hysteresis, marked as ΔT.

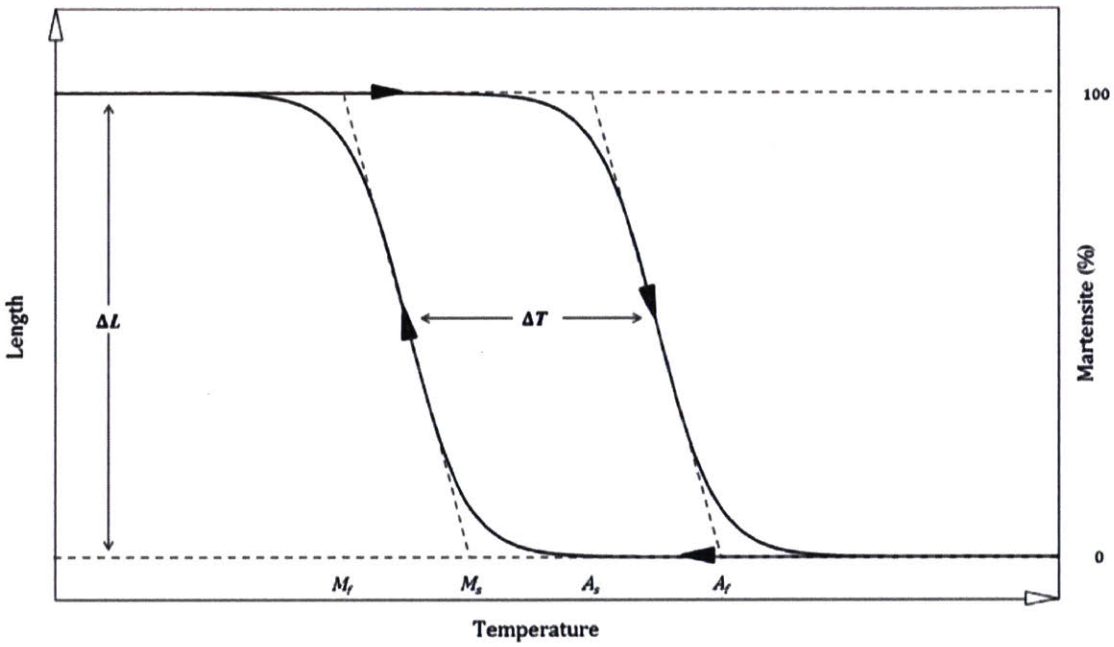

Figure 2-2: Thermal hysteresis of SMAs. [13]

The martensite structure is malleable due the low symmetry in its crystal structure, which can be arranged in different ways. The different crystal arrangements correspond to macroscopic deformations applied to the material [13]. When the transition occurs, all martensite variants transform into the only possible austenite crystal structure, recovering the memorized shape.

Fig. 2-3 represents the stress-strain-temperature space of the shape memory effect. When stress is applied, the material behavior is initially elastic (1-2), followed by an apparently plastic deformation characterized by the change of the variants of

martensite crystals to a single stable martensite crystal structure (2-3) and, after saturation, a second elastic deformation happens characterized by the elastic deformation of the new martensite microstructure (3-4). When the material is unloaded, the elastic deformation is recovered, but the apparently plastic deformation caused by the restructuring of the martensite crystals is maintained (4-5). When the material is heated to above its transition temperature, the martensite to austenite phase transition starts, allowing the material to recover its original shape (5-6-7). When the material is cooled, the initial state is finally reached (7-1).

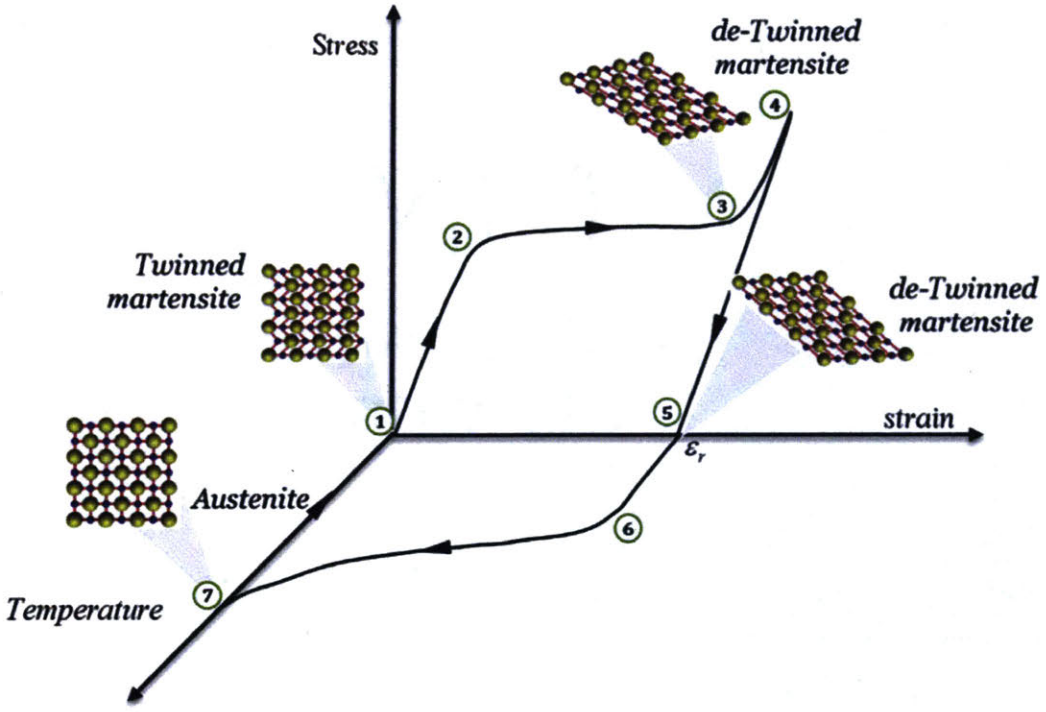

Figure 2-3: Shape memory effect on stress-strain-temperature space. [13]

Besides shape memory, SMAs also present pseudoelasticity characteristics (also called "rubber-like effect") [13], the property of completely recovering from significant deformations, as described in Fig. 2-3. Most metals cannot withstand much more than 0.2% deformation without entering the plastic regime, but SMAs can recover from up to 10% deformation without permanent shape changes.

The type of SMA considered in this thesis is the nitinol, an alloy with 53-57 weight percent (or 48-52 atom percent) of nickel and the remaining weight of titanium, a near equiatomic alloy [13]. The nitinol was developed in the US Naval Ordnance

Laboratory, also known as NOL – and hence the name: Ni-Ti-NOL. Other metal alloys that also present shape memory effects are copper based alloys, like Cu-Zn-Al and Cu-Al-Ni; and iron based alloys, like Fe-Pt and Fe-Pd. Between these options, nitinol is the alloy that shows the best shape memory effect, besides being corrosion resistant, very stable, and biocompatible, making it the most common SMA to date.

The transition temperature of nitinol ranges from -100°C to 100°C, it presents poor machinability, its density is of 6.4 kg/m^3, its Young modulus is 83 GPa in the austenite phase and 30 GPa in the martensite phase, and the maximum recoverable strain of nitinol is 8%.

SMAs are frequently used in the orthodontic and medical industries, but are still uncommon in the aerospace field. According to Lecce and Concilio [13], the main reason for this gap is that the SMAs fatigue characteristics have not yet been fully studied and the transition temperatures that are currently available might be too low for aerospace usage. While the fatigue performance still needs to be studied, there might be ways to work around the currently available transition temperatures. The next section describes some applications of SMAs that showed successful results.

2.2 Uses of SMAs as Actuators

Xin Lan *et al.* designed an SMA hinge to actuate a deployable antenna [12]. The 1.4 m diameter umbrella-type antenna was composed of a deployable truss of six radial ribs and a reflective membrane surface. Each rib had one SMA-actuated hinge in which a nitinol wire would be heated by joule effect, contracting and actuating the hinge, as can be seen in Fig. 2-4. The hinge showed to be easy to fabricate, reliable, compact, and lightweight.

Hartl and Lagoudas captured in a conference paper the aerospace applications of SMAs by 2007 [9]. The authors describe a Northrop Grumman project of a morphing wing that applied antagonistic SMA-actuated flexural structures that would change the wing profile during flight, improving the aerodynamic performance without adding significant weight. Sadly, the provided torque by the SMA was not enough

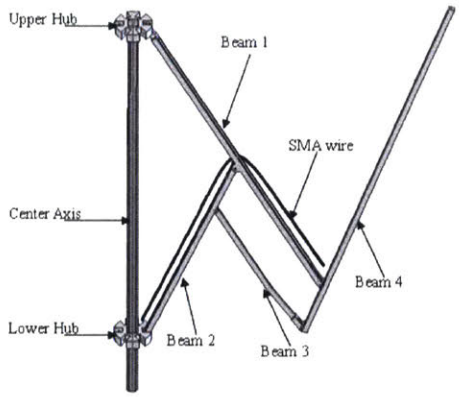

Figure 2-4: Deployable antenna actuated by a nitinol wire. [12]

to actuate the structure and large SMA component fabrication is not yet feasible, so the project was not successful. Hartl and Lagoudas also describe the SMA-actuated variable geometry chevron developed by Boeing for a GE90-115B Jet engine. The device optimized the chevron deflection, reducing noise during take-off and increasing efficiency during cruise flight. The provided integrated actuation performance met the design goals.

Hartl and Lagoudas also discuss the uses of SMAs as actuators in space [9]. The most common use is in low-shock release, substituting pyrotechnic release mechanisms. The trend of small satellites pushes for compact release devices, and the authors believe that SMA actuators can be an order of magnitude smaller than their off-the-shelf counterparts. The Lightweight Flexible Solar Array (LFSA) was a device developed by Lockheed Martin and NASA-Goddard to deploy satellite solar arrays using an SMA strip as the hinge – when heated and actuated, the SMA would open a previously folded solar array. The deployment worked and took only 30 seconds. The hinge can be seen in Fig. 2-5. The authors also cite the SMA actuator used in the Mars Pathfinder mission to expose a clean region to the sun and allow the measurement of the negative effects of dust settling on solar panels. Lastly, SMAs are also being used as actuators on inflatable structures, but some challenges in the thickness ratio between the SMA strips and the inflatable membranes are delaying the feasibility of this application.

Jani *et al.* wrote an extensive review on shape memory alloy research and ap-

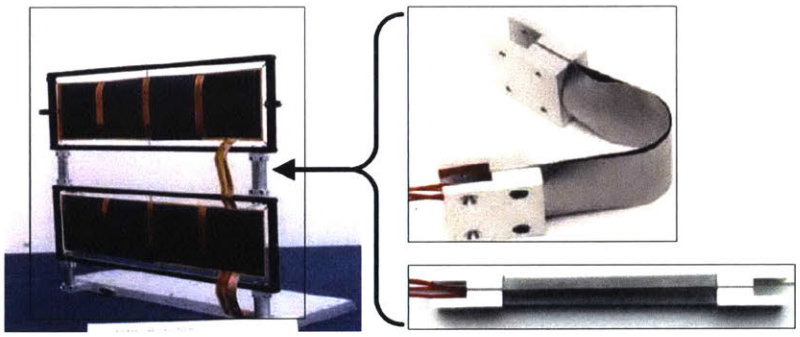

Figure 2-5: LFSA hinges in both folded and deployed configurations.[9]

plications in 2013 [10]. The focus was on SMAs as actuators used both in research and commercial domains in the automotive, aerospace, robotic and biomedical fields. They found more than 20,000 worldwide patents on SMAs and applications, and collected possible features of SMA actuators in Fig.2-6. The authors say that all these features represent opportunities to replace conventional actuators, such as electric motors, pneumatics and hydraulics, because of the significant reduction in mechanical complexity and size that an SMA actuator represents. Nitinol is also 25 times more work dense than electric motors and is able to lift more than 100 times its weight.

A big design challenge that Jani [10] describes is the low activation frequency of SMAs. These materials have relatively high heat capacity and density, which results in a slow heat transfer into and out of the SMA. Rapid heating can be achieved with a large heat dump on the actuator, but the cooling rate is limited by conduction and convection around the material, making fast cooling hard to achieve. Slow cooling rates mean that there is a large period between the end of an actuation and the beginning of the next one. Some strategies have been developed to expedite the cooling process, such as forced air convection, flowing liquids, using thermoelectric modules, applying heat sinks, and using conductive materials, but each technique has its own disadvantage, like high energy consumption, complexity, cost, or noise production. The authors also cite the need for fatigue studies as one drawback of SMA actuators. Jani *et al.* also described some uses of SMAs in the aerospace field [10] divided as actuators, structural connectors, vibration dampers, sealers, release or

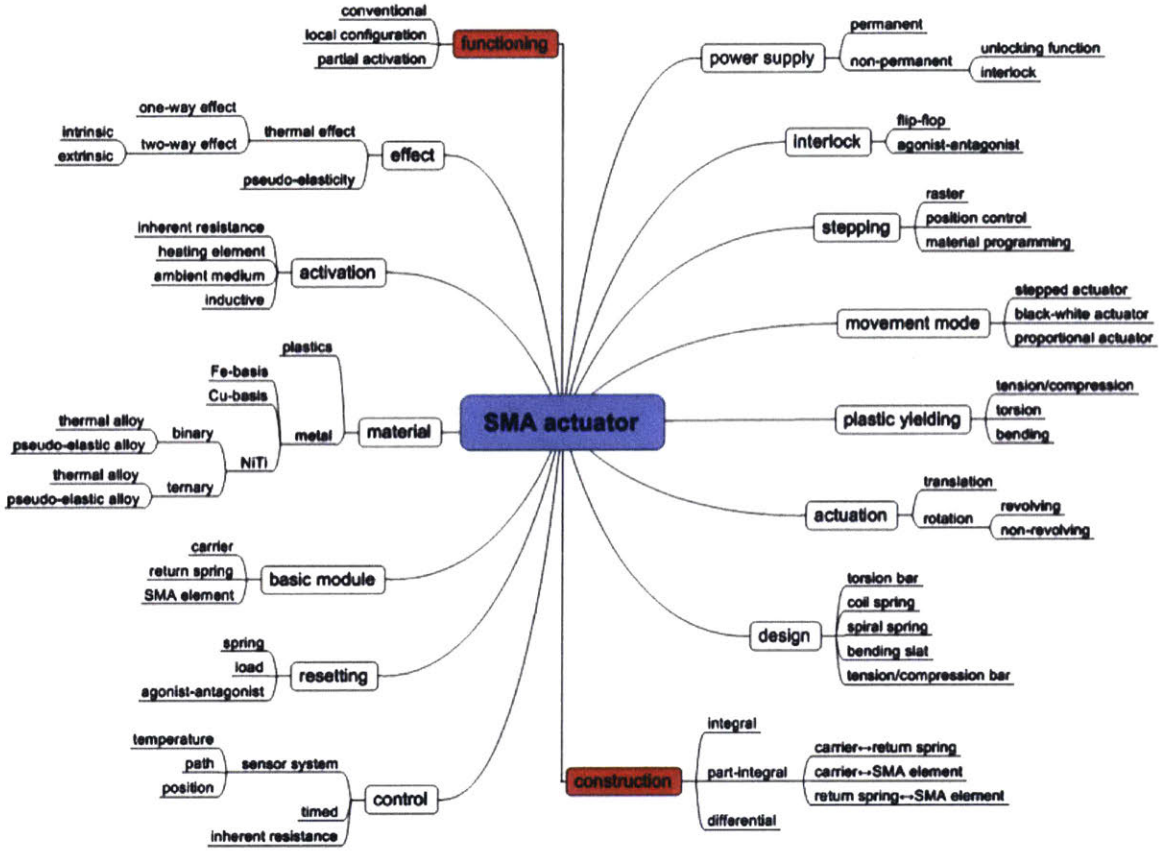

Figure 2-6: Possible features of SMA actuators. [10]

deployment mechanisms, inflatable structures, and manipulators.

Khatsenko wrote his master's thesis on a rotary SMA actuator for CubeSat deployable structures [11], with the goal of repeatably actuating a solar panel of a 3U CubeSat by 90°. The mechanism was a hinge that was purely composed of SMA strips, without any other guiding or supporting structure, as can be seen in Fig. 2-7. The chosen heating mechanism was the Joule effect. The shape of the SMA strips was rectangular to facilitate fabrication. The temperature of the SMA was measured by a hand-held infrared thermometer, the angle of deployment was estimated visually, and the control of the actuation was open loop. To achieve a repeatable actuation, the two SMA strips were trained to opposite directions and would actuate against each other. As can be seen in Fig. 2-7, Khatsenko was able to achieve the desired 90° actuation in the laboratory environment.

The literature on SMA use in space is promising and there is a tendency to also use

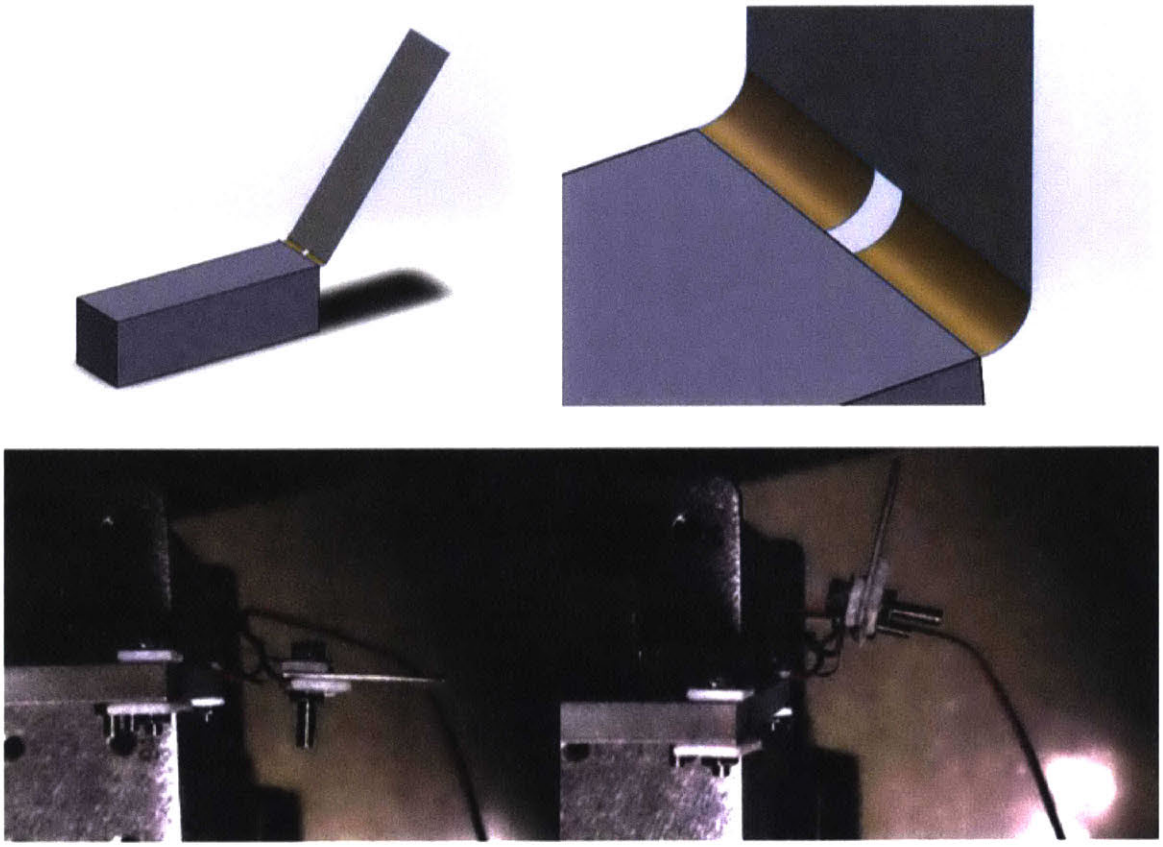

Figure 2-7: Drawing and picture of the SMA hinge developed by Khatsenko.[11]

SMAs as folding devices [9][10][11], not only as stretching/compressing mechanisms. SMAs are also entering the field of repeatable actuators [9][11], with hopes to replace electric motors in applications where size and weight are crucial [10]. There is even the possibility for SMAs to become precise actuators if good control strategies are applied. [2] Hence, the small and lightweight mechanical actuator to be developed in this work will use the folding memory of SMAs to precisely and repeatedly actuate an external surface, with applications such as solar panels of 3U CubeSats.

Chapter 3

Prototyping

To develop a small, lightweight, repeatable, and precise actuator based on SMA folding characteristics, four prototypes were made. This chapter describes the prototype evolution.

3.1 SMA Actuator Design

The actuator structure is a hinge, which needs to be able to actuate in two directions in order to be repeatable. Two-way SMAs exist, but they are not fully reliable as their fabrication techniques are yet to be perfected [19]. To allow this double actuation, two SMA strips are used in opposition to each other: one strip actuates to deploy the mechanism, and the other strip brings it back to the stowed position. The two strips can also be used in opposition to achieve a better position control. Fig. 3-1 schematically shows how the two strips actuate.

The shape of the SMA strips is chosen not only to optimize the bending force to bending resistance ratio and the bending direction bias, but also to allow a reliable and repeatable attachment of the SMA strip to the structural hinge.

The bending force of an SMA is derived from how much the material compresses or stretches as a function of its Young's Modulus, as can be seen in Eq. 3.1. The bending resistance of an SMA is derived from the beam deflection caused by a moment applied to the beam, as shown in Eq. 3.2. For this calculation, we assume that the

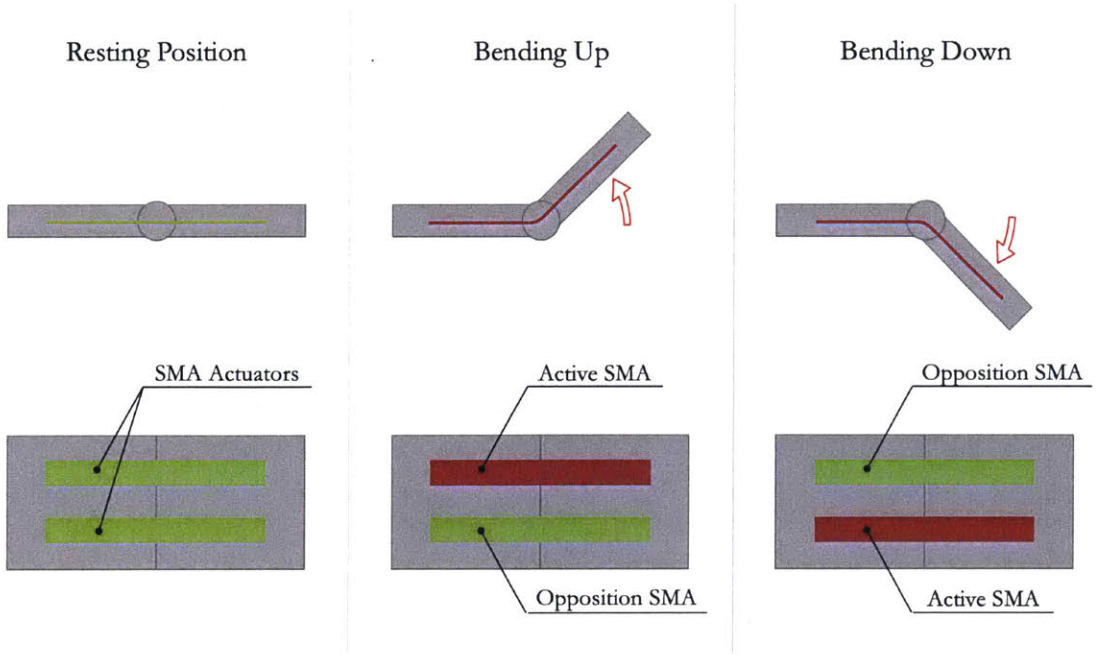

Figure 3-1: Schematics of the opposition hinging motion of the SMA actuators.

SMA behaves as a cantilever and weightless beam with the force being applied on the other end of the beam. This means that the force applied by the actuated SMA is proportional to the square of its thickness, whereas the resistance offered by the non-actuated SMA is proportional to the cube of the thickness:

$$F_{applied} = AE\frac{\Delta L}{L_0}\sin(\alpha), \tag{3.1}$$

$$F_{resistance} = \frac{Eb\delta}{4}\left(\frac{h}{L_0}\right)^3, \tag{3.2}$$

where A is the cross-sectional area of the actuator, E is the Young's Modulus of the SMA, L is the length of the actuator, α is the actuation angle, b is the width of the cross-section of the actuator, and h is the height of the cross-section of the actuator. Aiming for maximizing the applied force with respect to the resistance force, the actuator developed in this work has the smallest possible thickness that is still strong enough to move the hinge: around 0.25 mm.

The second important parameter is the directional bias. The force necessary to bend any structure is proportional to the Young's Modulus of the material and the

second moment of area of the cross-section that is being deformed. This means that a round cross sectional area is equally bent in all directions, while a flat strip bends a lot easier on the direction of minimum thickness when compared to the direction of maximum thickness, as schematically explained in Fig. 3-2. The second moment of area of a rectangular cross-section is calculated through Eq. 3.3, where b represents the base of the cross-section and h represents the height of the cross-section.

$$I = \frac{bh^3}{12} \tag{3.3}$$

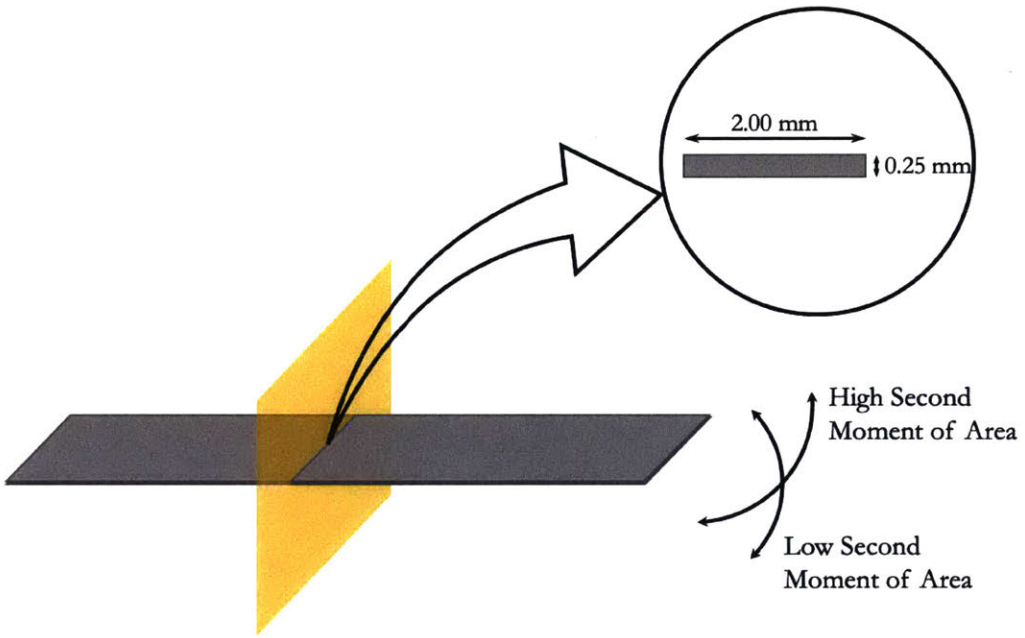

Figure 3-2: Schematics of the cross section of the SMA actuator.

In a rectangular cross-section, the desired bending is in a specific direction, which gives preference to the flat strips. The strips are also easier to assemble, as one can easily tell assembling directions is (which does not happen with round wires).

The third important parameter that is into account on the actuator design was the attachment of the actuator to the hinge. SMAs are known for their poor solderability [19], especially when significant current is going to pass through them. Round wires are more difficult to strongly and reliably attach to any structure, as SMAs stretch substantially during actuation and can come loose of compression-based and friction-

based attachments. The wires are also of small diameter (less than 1 mm), so it is not possible to machine holes through them. The flat strips, on the other hand, can easily be drilled, allowing for a simple bolt and nut attachment. This type of mounting also has the advantage of electrical conduction. Due to the higher second moment of area, the round wires tend to actuate with more force and quicker than the flat wires, but it is also harder to actuate against them making it difficult to work in opposition and to stow back the actuated surface.

The current design is a flat strip with a small thickness (ranging from 0.15 to 0.5 mm) and with holes on the ends for bolt-nut attachments to the hinge and the electric circuit, as can be seen in Fig. 3-3.

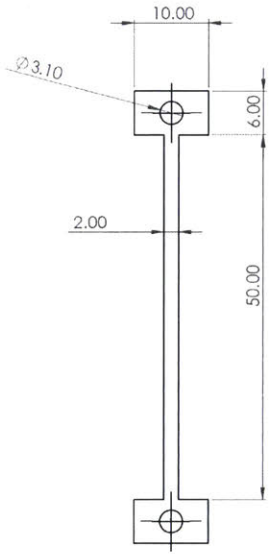

Figure 3-3: Final design of the SMA actuator.

To train the SMAs to their desired shape, they are annealed at 500 °C for around 30 minutes. The exact annealing time changes slightly as a function of the thickness of the strip: the 0.25 mm thick strips took 25 minutes to be annealed, whereas the 0.5 mm thick strips took 35 minutes. The oven was maintained at 500 °C constantly at the MIT Glass Lab, and the doors would be quickly opened for the SMAs to be inserted and, later, for them to be taken out. Slow cooling rates decrease the ability of the SMAs to achieve their desired shape, so right after taking the strips out of the oven, they had to be quenched in cold water. To address this issue, four different

types of mold lids were designed and machined: closed lid, lid with one slot, lid with two slots, and lid with four slots, as can be seen in Fig. 3-4. The best actuation was achieved when the quenching was performed with the lid that had four slots, confirming that the quenching speed is important for the complete annealing of the SMA. This annealing method was chosen because it seems to be a good trade between speed of annealing and final actuation properties. Other options would be putting the SMA on the top of a burning flame or short circuiting it.

Figure 3-4: Different lids tested for better quenching.

Even with good quenching, the strips do not completely recover the trained shape when they are acting against an opposing force, so they had to be trained to a higher bending angle. To determine what would be the best over-training angle that would allow a 90° actuation, we made an array of tests: we designed and machined annealing molds with different bending angles: 90°, 120°, 160°, and 180°, as can be seen in Fig. 3-5.

Four SMAs of the same thickness and shape were annealed for the same period using the four different molds. The 90° bent SMA was not able to recover the full 90° angle even when no opposing force was being applied to it. The 120° and the 160° bent SMAs were capable of recovering above the 90° threshold, but would not reach that angle when a small opposing force was applied. Lastly, the 180° bent strip showed the best performance. Hence, the strips used on the project were trained at 180° bending to be able to achieve the desired 90° actuation in each direction.

Another important detail on SMAs is their maximum bending limit. As previously

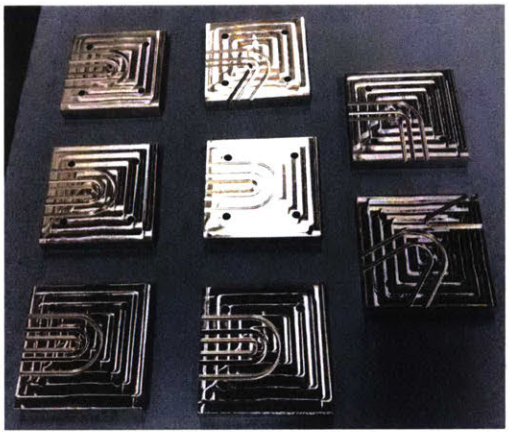

Figure 3-5: Different molds tested for the over-training of the SMA.

explained, SMAs cannot recover when there are strained to more than approximately 10% of their thickness [13]. To be able to test different thicknesses of strips, the molds were designed with three different *U-shaped* rails, each one with a different bending radius to be able to train different thicknesses of SMAs.

3.2 Hinge Design

The actuation mechanism is comprised of two SMA strips as actuators and one hinge as guidance structure. The hinge was designed to match the actuator shape that was described in Section 3.1, namely a flat strip of 2 mm width, 50 mm of actuation length, and thicknesses ranging from 0.15 mm to 1 mm.

The hinge is designed such that the midplane of the SMA strip is located on the neutral axis of the hinge, as illustrated in Fig. 3-6. As the bending axis passes along the midplane of the strip, the deformation on the tensioned and on the compressed sides of the strip are minimized. To achieve the midplane positioning, the hinge had the SMA strip on the middle of its thickness. This design decreases the presence of extra strain and buckling on the SMA, as will be described in Chapter 4.

It is important that the SMA strip is constrained just enough to be forced to follow the hinge's neutral axis without overconstraining its position. An extra piece

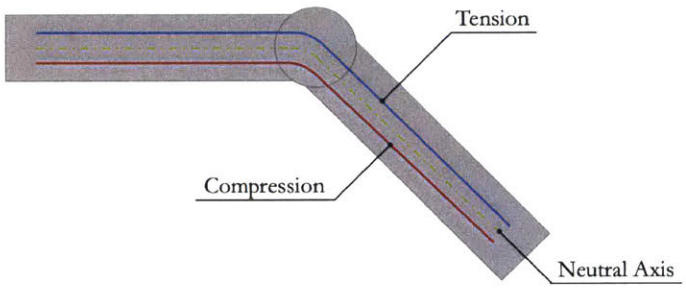

Figure 3-6: Schematics of the compression and tension around the neutral axis of the hinge.

was then added on the top of the strip, close to the bending axis, to maintain the strip as close as possible to the hinge. These were called "buckling straps", as illustrated in Fig. 3-7. One end of the SMA strips is bolted to the hinge and to the cap of the model CubeSat used in the laboratory to perform the experiments. The other end is bolted to the surface that is being actuated. In Fig. 3-7, there is no such surface, but a model of a CubeSat solar panel was used to perform the hinge characterization tests to provide the momentum and inertia in similar levels than what would be encountered in an actuation application. The buckling strips are also bolted to the hinge and to the underneath surface – either the CubeSat cap or the actuated surface.

The bending axis of the hinge is composed of a dowel pin, a bushing, and a retaining ring. The hinge structure was 3D printed in high-temperature resistance, insulative plastic and the central holes on the bending axis were reamed, where the bushing was then press-fitted. The other end of the bending axis was also reamed and the dowel pin was press-fitted. The two sides of the hinge were then assembled, resulting in a low friction hinging mechanism, as can be seen in Fig. 3-7. Both sides of the hinge are symmetric, making it easier to fabricate and assemble.

Fig.3-7 also shows, on the top, the encoder mount. A magnetic encoder is used to measure the angle of the hinge without adding friction to the mechanism. The magnetic piece was inserted in the moving part of the hinge, and the reader piece was inserted in the designed mount. No influence of the magnet on the hinge performance was noticed. The data from the encoder was used to characterize and control the bending of the hinge, as will be described in the results section.

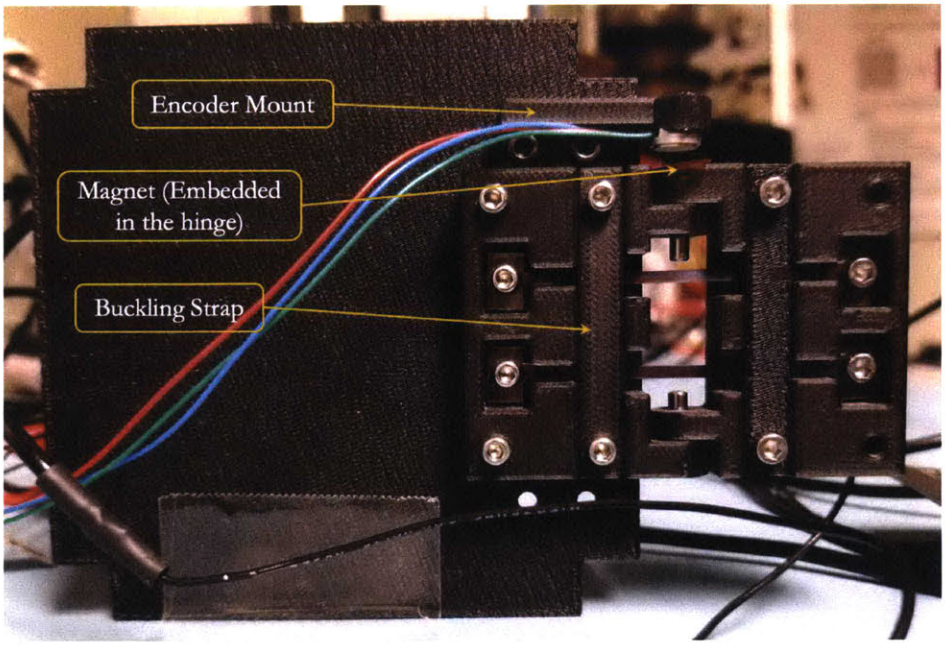

Figure 3-7: 3D-printed model of the current hinge design.

3.2.1 Design Exploration

Other design options have been studied, like using SMAs as springs and stretch/compression mechanisms instead of bending actuators. There have also been prototypes of four-bar mechanisms that would amplify the actuation angle of a hinge though SMAs, but those are more mechanically complex systems, deviating from the main simple-use proposal of this work.

There is also another prototype being designed that uses round wires instead of flat strips. The advantages of the flat strips over the round wire have already been discussed, but one main disadvantage is the lower actuation force density for the strips. Due to the higher second moment of area that the wires have at the same cross-sectional area of the strips, they can overcome buckling and stretching issues more easily. Round wires are also more common, being easier to acquire for frquent tests.

3.3 Building

The alloy chosen for our tests was nitinol, an alloy of nickel and titanium at near equiatomic mixture. The chosen transition temperature was 80 °C. The material was acquired from Kelloggs Research Labs in the form of small plates with the desired thickness, but with 25 mm width and 150 mm length. The desired actuator shape was then machined out of that stock by ourselves.

It is interesting to note that machining SMAs is a tricky process. Both laser cutting and sanding generate a significant amount of heat, which has shown to degrade the performance of the SMA. Milling at the right feeds and speeds with coolant does not significantly degrade the material [16], but requires special mounts and substantial amounts of fluid, making it an expensive process. The best option we could find is to cut the parts through water jetting. This process does not degrade the material properties, but it also does not present high precision, contributing to the variation of resistance between the SMA strips.

The SMA is too thin to be directly water jetted, so it was mounted to an aluminum base and held to it using aluminum tape. Each SMA plate was large enough for four strips to be made, leaving some extra space for smaller strips used to test the annealing process. Fig.3-8 shows the aluminum base, the SMA plate, and the actuation strips after they were water jetted.

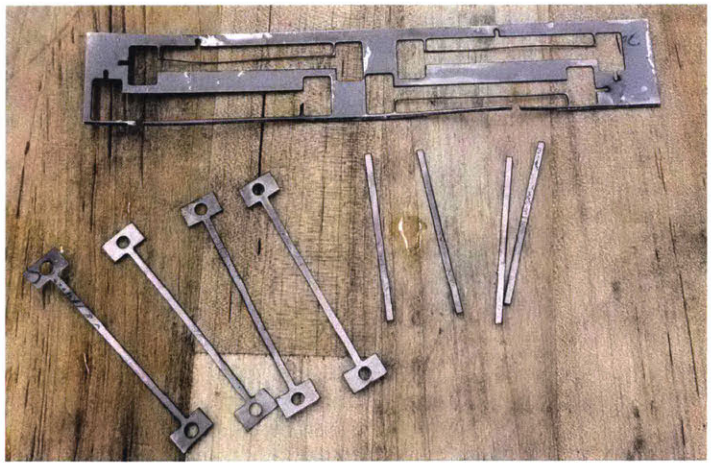

Figure 3-8: SMA actuators cut from the original sheet through water jetting.

As previously stated, the hinge was 3D printed out of a high-temperature resistance material: a mixture of nylon and carbon fiber (named Onyx, a proprietary blend from Markforged), resulting in a melting temperature of 240 °C. Other materials were also tested, such as ABS and PMMA resin, but they could not withstand the heating of the SMA strip without slightly melting.

The parts of the hinge that needed a better precision than what the 3D printing process could offer were reamed after the piece was ready. A press was also used to insert the bushings and dowel pins, as described in Section 3.2.

The last building process was annealing the SMA strips, which was performed in the MIT Glass Lab. The air composition during annealing was not controlled, which resulted on the formation of oxides on the surface of the SMA. Oxides have a low electrical conductivity, increasing significantly the resistance between the SMA and the bolt through which the power was being applied. Two approaches were taken to solve this problem: sanding and coating.

Sanding the strips after they were annealed is a simple and cheap solution, but it results in some heat to the SMA, degrading its bending capabilities. Sanding under water resulted in less heating, but was still suboptimal. The second solution, coating, was attempted only once. One SMA strip had its ends gold plated before being annealed. The coating avoids the formation of oxides, eliminating the need of sending the strip and theoretically increasing the quality of the electrical contact. Sadly, the gold plating of the nitinol strip was not successful: besides not adhering properly to the nitinol surface, the coating also increased the electrical resistance between the SMA and the bolts. We are still trying to understand the reasons for the low adhesion. Although sanding the ends of the SMA strip under water could still slightly damage the material, it was the best way to date to eliminate the presence of the oxides. Hence, the strips used in the tests were sanded under water.

3.4 Control and Electronics Schemes

Most of the electronics and control algorithms were developed by the undergrad research students Charles Linday, Mario Contreras, and Shreeyam Kacker. Charles is a Class of 2021 Aeronautics and Astronautics MIT student, Mario is a Class of 2019 Mechanical Engineering MIT student, and Shreeyam is a Class of 2020 Aeronautical Engineering visiting student from Imperial College London. Their work is briefly described here. More information can be found at Mario's bachelor thesis [2] and Charles' research report (unpublished, but available upon request).

The electronics are designed to deliver the proper power to the SMA strips through Joule heating effect. The printed circuit board (PCB) inputs power from a Rigol power supply and tunes the voltage to 1.8V and 5V to also drive the magnetic encoder, the Arduino computer, and an accelerometer. The voltage input is in the form of a duty cycle, which is applied to a MOSFET to switch the power on and off over a shunt resistor connected in series with the SMA. From the voltage readings and the shunt resistance, the current on the SMA can be calculated. The power that is applied to the SMA is then calculated from the voltage and current flowing through it. The resistance of all the wires and connectors are accounted for in the calculations, which is an important step, as the SMA resistance is on the same order of magnitude as the wires. The controls and calculations are programmed into the Arduino, which also logs the power data that is going to be used in the controlling scheme. Fig. 3-9 shows the overall electronic schematic on the left and the PCB with the Arduino on the right.

The controller goals were to minimize the overshoot and maximize the actuation speed. The actuator should be able to reach a set point within 20 seconds and should avoid using the two SMA strips to reach the desired position to avoid the need of heating up both strips. It was assumed that for small power inputs the transfer function is linear time invariant (LTI), allowing the use of linear control theory.

To determine the transfer function of the hinge, the step response of the actuation angle was measured at a constant duty cycle command from the Arduino. As the

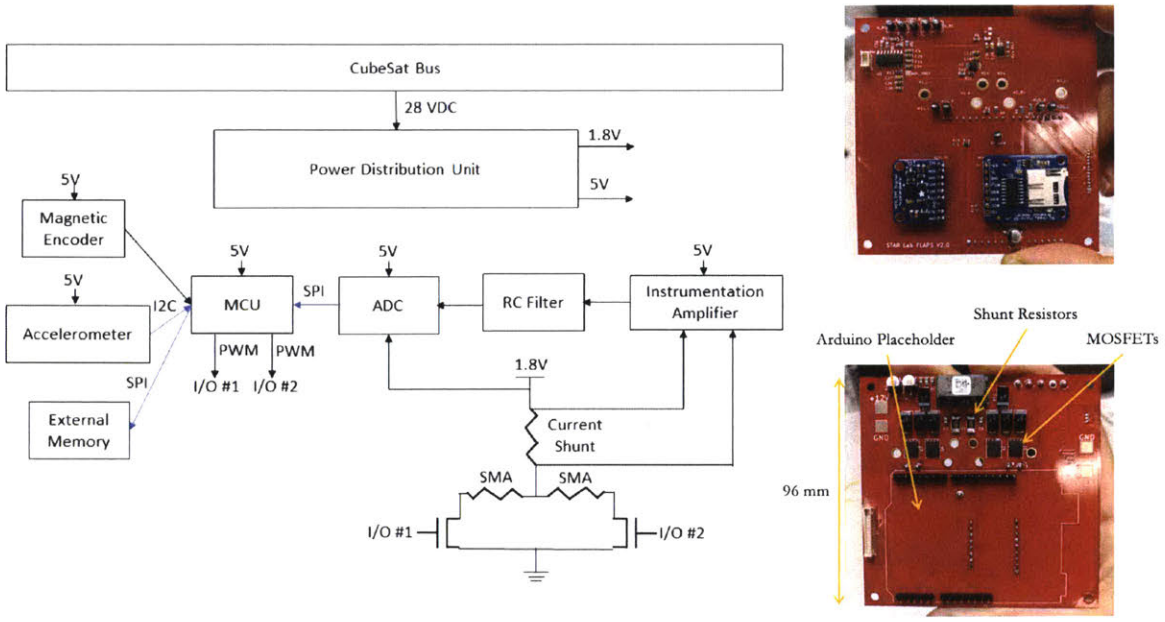

Figure 3-9: Electronic schematics on the left and actual PCB on the right. Image credit: Charles Lindsay.

SMA resistance changes when it heats up, the power signal on the SMA strip also changes. 25 tests were performed: 5 repetitions at each of 5 different duty cycles. Fig. 3-10 shows the measured power and angle as a function of time for one the tests, with 40% duty cycle.

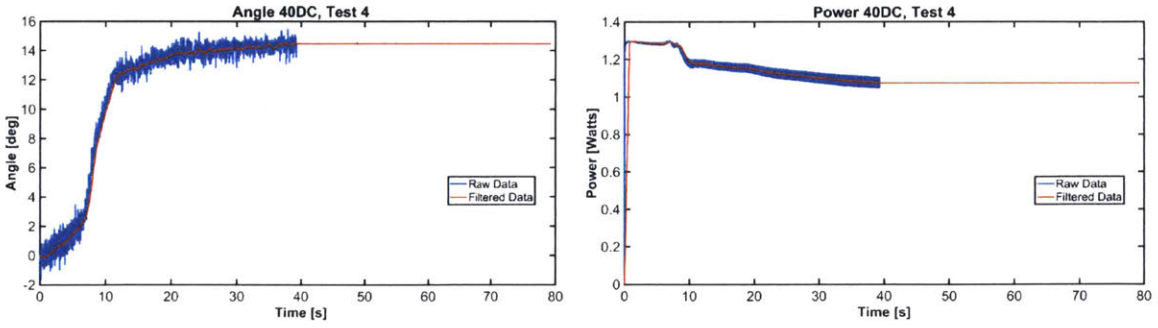

Figure 3-10: Power and angle measurements from a step response. Image credit: Mario Contreras.

The filter used in Matlab to smooth the data is a moving-average with 200 samples. The transfer function is initially assumed to be a pure second order system with two poles. Initial tests showed that there was a delay in the actuation due the warming

up of the SMA, until it reaches the transition temperature and the actuation starts. The lag was added to the transfer function, but the increased complexity only slightly affected the accuracy of the function. Hence, even knowing there is an unrepresented lag, the transfer function used was a pure second order, as can be seen in Eq. 3.4: [2]

$$\theta = \frac{1.144}{s^2 + 0.183s + 0.01597}, \tag{3.4}$$

where θ is the actuation angle and s is the frequency domain in the Laplace space transformed from the time domain in the physical space.

Lastly, the controller used in the Arduino was a proportional-integral-derivative (PID) control. The gains were found by auto-tuning the average test data using Matlab's response time algorithm and adjusted by a root locus tuning. The encountered gains were: $K_p = 0.04379$, $K_i = 0.002789$, and $K_d = 0.1442$. The schematics of the control system can be seen in Fig. 3-11.

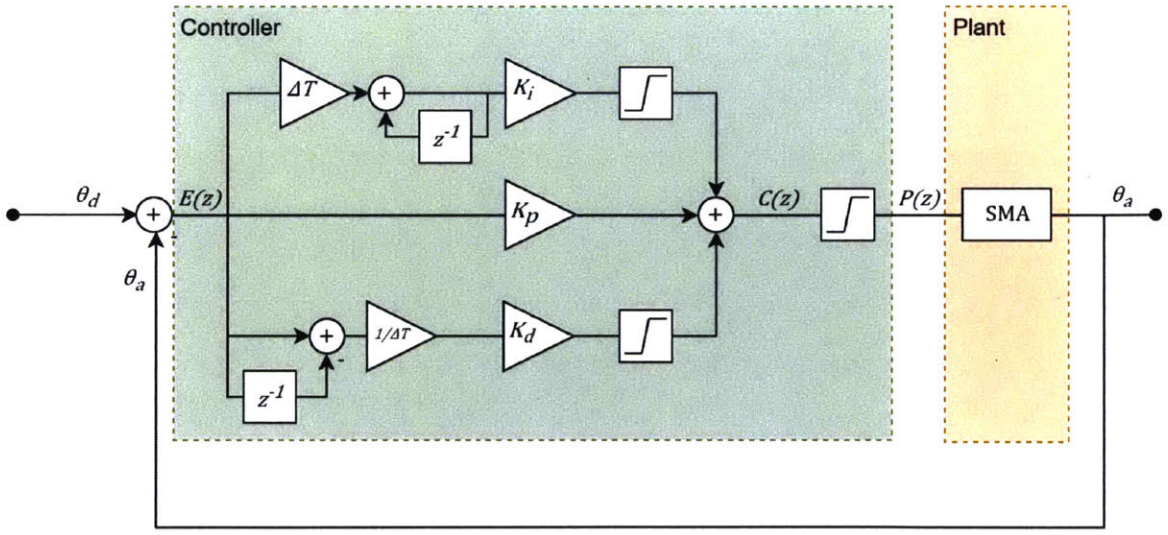

Figure 3-11: Schematics of the PID controller. Image credit: Shreeyam Kacker.

3.5 Parabolic Flight

The prototype is going to be tested in a parabolic "zero gravity" flight in the summer of 2019. The flight provides a reduced gravity environment and an increased gravity

environment up to 1.8 g during the flight parabolas [4]. The main goal of this test is to verify how the weight of the panel influences the hinging capabilities and responses of the designed actuator.

The parabolas performed by the airplane characterize four different gravity environments:

- Hyper gravity: up to 1.8 g for 60 seconds;
- Martian gravity: 0.38 g for 20 seconds;
- Lunar gravity: 0.16 g for 20 seconds;
- Zero gravity: 0 g for 17 seconds.

Each parabolic cycle is defined by one hyper gravity period followed by one of the low gravity periods (either 0, 0.16, or 0.38 g) [4]. The flights generally last approximately two hours and perform 20 parabolic cycles. The cabin pressure altitude is 8,000 ft and the temperature is maintained at approximately 80 °F.

The airplane is equipped with both AC and DC power outlets. Our experiment is going to be connected to the 115V AC outlet, which provides 20 Amps – one quarter of our consumption estimation.

The mechanical interface with the airplane inner structure is going to be made by an aluminum base plate that is attached to the floor through 6 3/8" bolts. The base plate hosts an aluminum and acrylic box that encapsulates the entire experiment to provide flight safety. The CubeSat model with the hinge prototype and the model solar panel are contained in the box for safety reasons, as can be seen in Fig. 3-12.

The interface between the user and the prototype are the purpose-built electronic boards and switches. Besides the previously described PCB, the flight box also has a PCB with 4 LEDs that indicate which SMA strip is being actuated and in which direction the hinge is moving. There are also two switches, one potentiometer, and one emergency stop button, that will kill the power to the experiment when pressed. The potentiometer will allow the user to set the desired actuation angle. The two switches will turn the experiment on and off, will allow manual input to the controller,

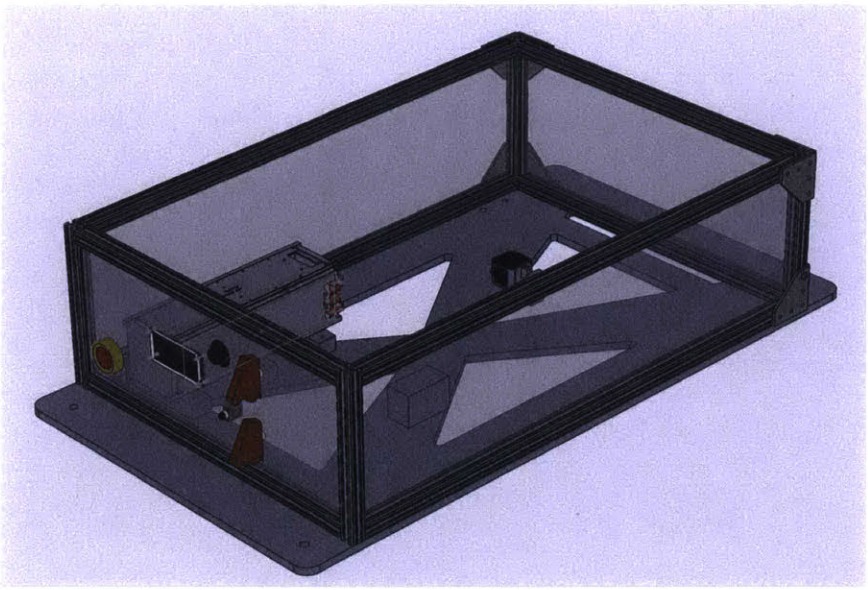

Figure 3-12: Safety box and interfaces for the Zero G flight.

and will a secondary back up hinge to be used instead of the main one in case it fails to actuate.

The concept of operation for the flight can be summarized in the following steps:

1. Prior to each parabola: Power management check to ensure all sensors are recording and the experiment is in a safe set up.

2. During each parabola:

   (a) Open the box cover, remove the solar panel foam holder, and close the box cover;

   (b) Set the actuator angle to the desired degrees value;

   (c) Arm the actuator;

   (d) Verify that the LEDs indicate actuation;

   (e) Open the box cover, place the solar panel foam holder, and close the box cover.

3. After each parabola: make sure the user reaches a safe position for the hyper gravity period.

The 5 initial parabolas are going to be used to ensure the experiment is working and to allow the user to acclimatize to the unusual environment. The following 14 parabolas are going to be used to effectively test the actuator, opening the the solar panel to a different set angle at each parabola. The final parabola is reserved for any troubleshooting that becomes necessary during the flight.

After the flight, the time of actuation, the actuation angle, and the control precision of the hinge in flight are going to be compared to the ground results to evaluate the effect of the panel weight on the hinge dynamics.

Chapter 4

Results and Discussion

The final results from this work are still ongoing, as the main tests are going to be performed in the parabolic flight in the Summer of 2019. Prior to flight, ground tests are performed to characterize the hinge assembly and study the design. The following sections describe the lab set up and the test results.

4.1 Viability Tests in the Lab

The viability tests were performed in the Space Telecommunications, Astronomy and Radiation Laboratory at MIT. Three main sets of tests and simulations were performed: force estimation, actuation angle, and control response.

4.1.1 Force Estimations

As explained in Section 3.1 and Equations 3.1 and 3.2, the bending force of an SMA is derived from its Young's Modulus formulation, while the resisting force against its bending is calculated through the beam deflection formulation. The bending force for a 0.25 mm thick strip is calculated using Eq. 3.1 and the results can be seen in Fig. 4-1 for the bending force as a function of the power level and the actuation angle.

To validate the calculations, some simple tests were performed to measure the force applied by a bending SMA strip. The first batch of tests was performed with

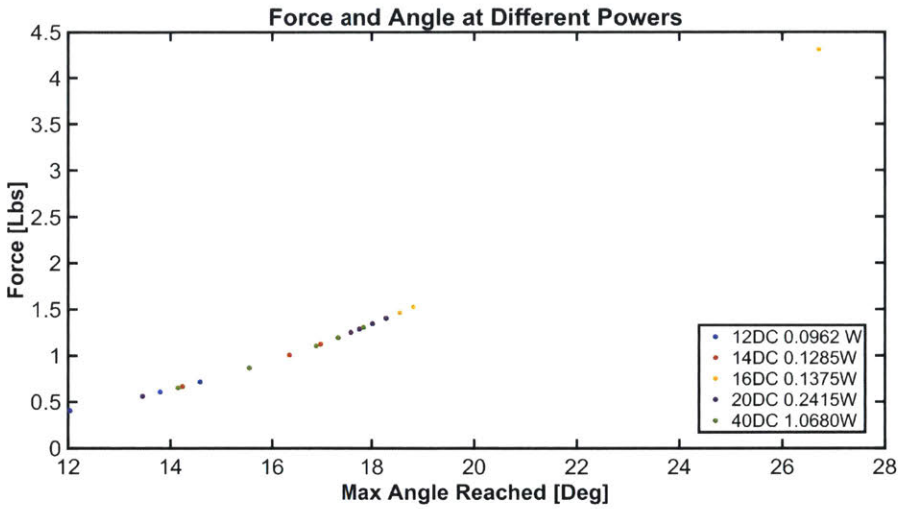

Figure 4-1: Estimation of the bending force at different power levels and actuation angles. Image credit: Mario Contreras.

a small scale, rated for a maximum of 3 kg with measurement uncertainties on the order of 0.1 g. A mount for the SMA strips to hover over the scale was designed and built, as can be seen in Fig.4-2. The SMA was mounted with one side on the mount and one side hanging. Both ends were attached to a power supply that ran 1 W of power through the strips.

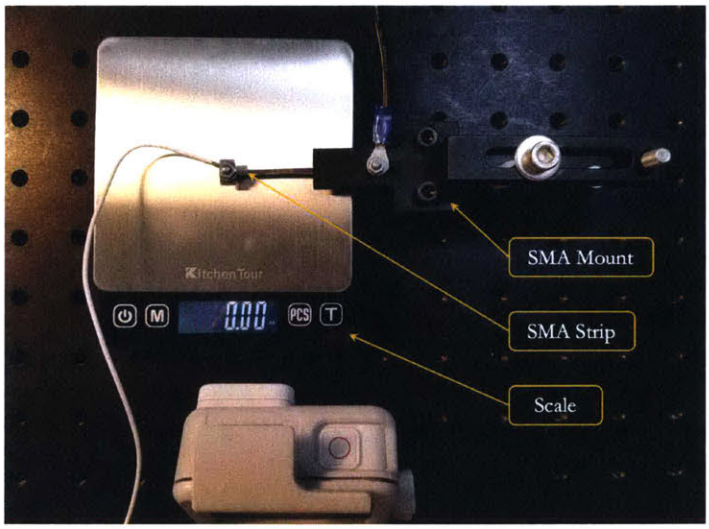

Figure 4-2: SMA bending force measurement using a scale.

There was some uncertainty on whether the weight of the leads and screws would influence the scale readings, so another set up was prepared using a Futek load cell

as a measurement unit. The load cell was hung from one end and the opposite end was connected to the hanging side of the SMA, as can be seen in Fig.4-3.

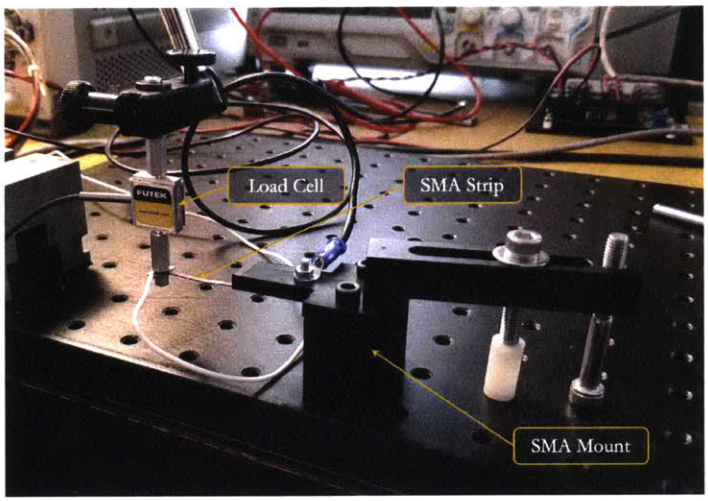

Figure 4-3: SMA bending force measurement using a load cell.

Two different thicknesses of SMA strips were tested: 0.25 mm and 0.5 mm. Both were tested in the position guided by the mounting, namely, approximately 15°. The average force of both the scale and the load cell measurements for the 0.25 mm thick strip was of 1.4 lbf, whereas the average force of both the scale and the load cell for the 0.5 mm thick strip was of 3.2 lbf.

From the plot in Fig. 4-1, the expected bending force of the 0.25 mm thick strip at 15° is approximately 0.9 lbf, which is similar to the value measured in the experiments. The calculations and the experiments are not extremely precise, but having similar results is encouraging and supports the ballpark estimation.

From Eq. 3.2, the force necessary to bend the nonactive SMA strip can be calculated based on the material and tested geometry. The Young's Modulus being used is the one from the martensite state of the SMA. The bending will occur while the SMA is cold, which is between 28 and 40 GPa. The width, the thicknesses, and the length of the strip are known, and the deflection can be calculated from the experimental set up. The resulting force required for bending is thus approximately 0.23 lbf for the 0.25 mm thick strip and 1.80 lbf for the 0.5 mm thick strip.

The comparison between the necessary bending force and the provided bending

force for both thicknesses can be summarized as:

- 0.25 mm thick: provides 1.4 lbf and needs 0.23 lbf to be bent;
- 0.5 mm thick: provides 3.2 lbf and needs 1.80 lbf to be bent.

Fortunately, both thicknesses of SMA strips provided more bending force than necessary. As previously stated, the ratio between provided actuation force and necessary non-active force is more favorable for the smaller thicknesses, but the absolute force difference was larger in the thicker 0.5 mm strip. This opens some room for discussion, as different characteristics can be more valuable for different applications. In this study, focus was given to the 0.25 mm thick strip. Both thicknesses of strips showed problematic buckling and saturation angle behavior.

4.1.2 Control Response

The average of the 25 tested step responses measured at 5 different duty cycles are shown in Fig. 4-4. Each of the five power levels is an average of 5 tests and the line was smoothed by a moving average of 200 points, sampled at a rate of 285 Hz.

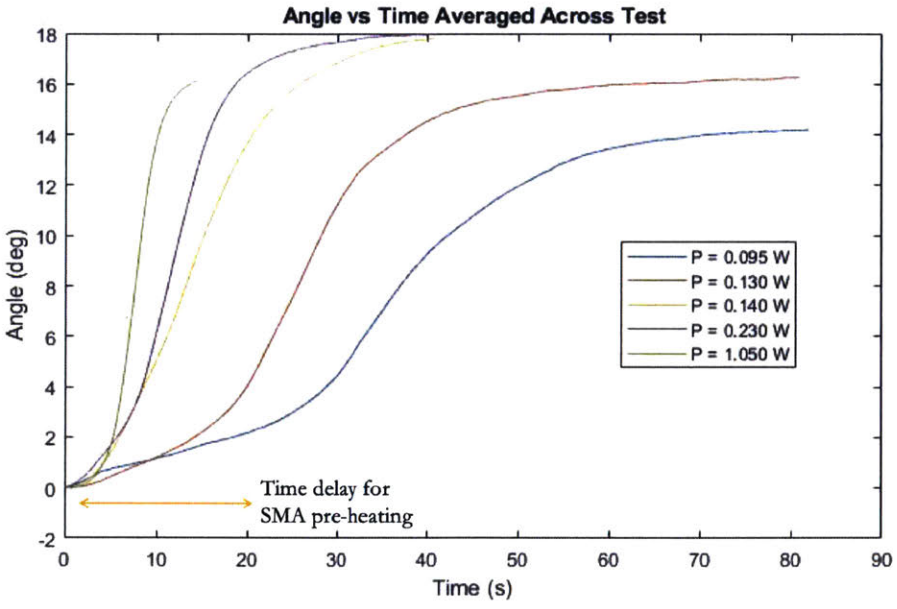

Figure 4-4: Average step response angle data for different power levels. Image credit: Charles Lindsay.

The initial low slope angle is caused by the time it takes for the SMA to heat up to its transition temperature. From the figure, if the time delay is ignored, the output angle is linearly proportional to the input power for low power levels up to approximately 18°. If the pre-activation temperature is controlled, then the system can be actually considered linear, time invariant up to 18° [2].

The controller gains were calculated as described in Chapter 3. Unfortunately, there was a conversion issue in the Arduino, resulting in a much lower output power than anticipated. [2] Initial tests were run with a set point of 20° with gains 50 times greater than the calculated values and about 0.14 W of input power, both with and without pre-heating the SMA strip to just below its transition temperature. Both tests resulted in an actuation so fast (less than 15 seconds) that the overshooting was unavoidable. The overshooting on the pre-heated test, though, was significantly smaller (on the order of 3° instead of 17° for the non-heated case). It is important to note that overshooting would require an actuation of the opposing SMA strip to decrease the actuation angle, which would imply in a second delay to account for the heating up of the second SMA.

A follow up test was performed with the same set point (20°) with gains 10 times greater than the calculated values. The overshot was satisfying, only up to 2°, but the actuation time was too long: about 75 seconds. [2] Fig. 4-5 shows the actuation angle as a function of time for this test. For applications in which a slow actuation is not a problem, this could be a good control solution.

Other set points were tested with both the 50 times and the 10 times higher gains. They all showed the same pattern of actuation: less than 15 seconds, but with overshoot for the 50 times gain; and more than one minute, but almost no overshoot for the 10 times gain [2].

4.1.3 Actuation Angle

From the different angles achieved with different powers in Fig. 4-4, one can tell that for up to approximately 0.15 W of power input the angle response is indeed linear. When the power is increased above that point, the linearity of the system

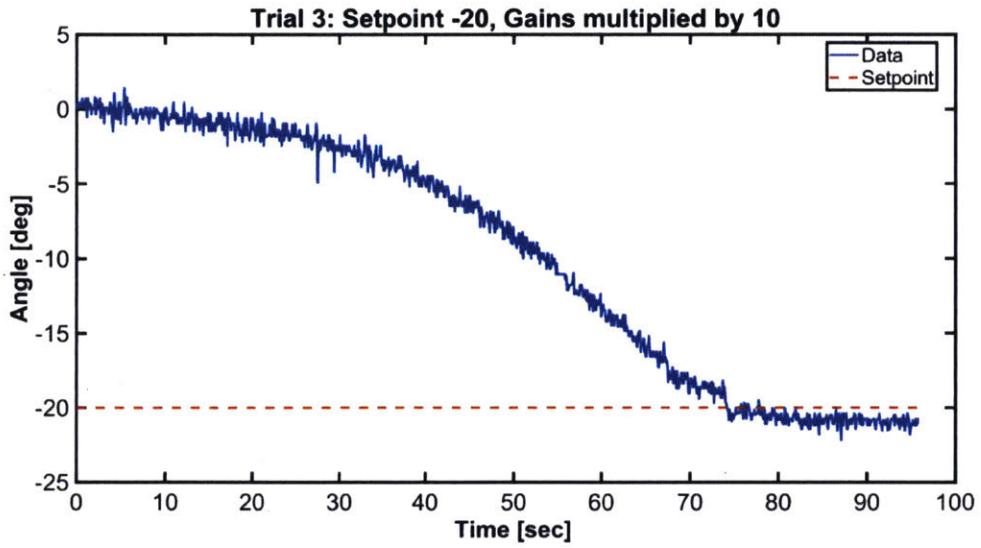

Figure 4-5: Gain tuning for control precision with 0.14 W input power. [2]

is lost. That is not directly due to the power input, though. The nonlinearities are introduced by what is going to be called a "saturation angle" achieved by the hinge. For the high gain, the hinge did move a little above this saturation angle. This probably means that there is still some room for extra hinging motion if the power input is increased. The maximum power tested was approximately 1.1 W. More tests need to be performed to fully understand this saturation.

The saturation at approximately 18° is due to the overconstraining of the SMA strips inside the hinge assembly. The strips are bolted on both ends and the hinging movement is guided by the pin and the hinge geometry, preventing the SMA from adjusting its length as it stretches and compresses when actuated. The bending movement also creates tension and compression at opposite sides of the SMA strip, as shown in Fig. 3-6. The small thickness of the SMA strips and their positioning on the neutral axis of the hinge minimize the amplitude of these spurious tensions, but do not completely eliminate them, making it problematic in an overconstrained assembly. More details on how this problem is being tackled can be found in Section 4.2.

4.2 Design Challenges

The main design challenge is the overconstraining of the SMA strip on the hinge. The unaccommodated tension and compression that results from this issue makes the non-activated strip of SMA buckle. When the strip buckles, it creates a significant resisting force against further movements of the active SMA, making the resisting force greater than the actuating force. The range of motion is then limited by this lack of net force availability. Fig. 4-6 shows a situation in which the top strip was trying to bend the hinge forward, but the bottom strip buckled against the movement.

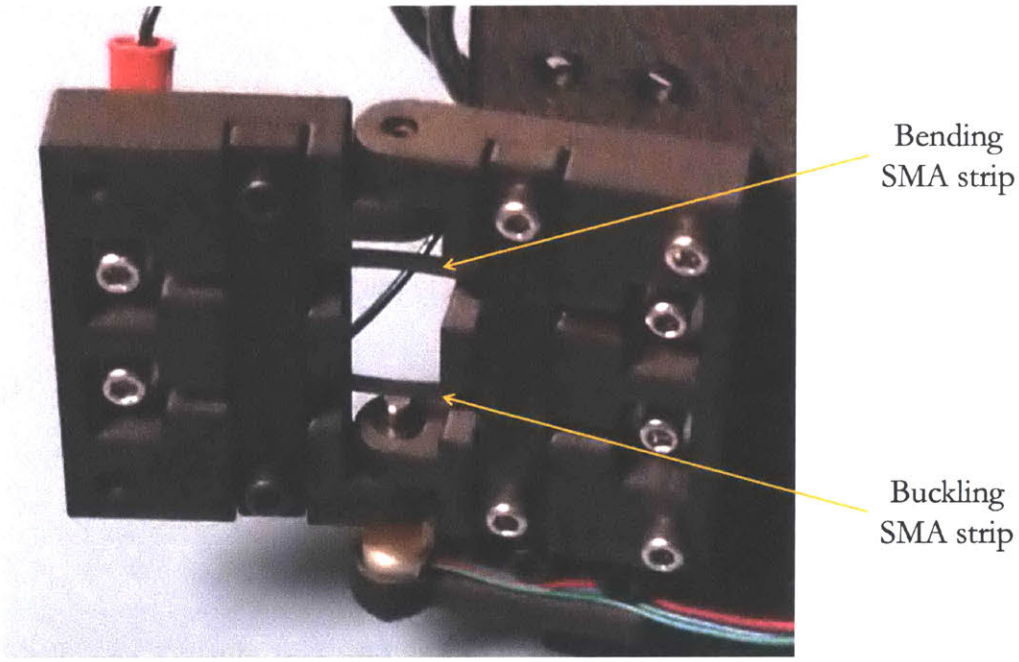

Figure 4-6: Example of an actuation in which the bottom SMA strip was buckled while the top SMA strip was being active.

To tackle this problem, we are routing into two possible solutions: eliminating the overconstraint and replacing the flat strips with round wires.

The round wires have previously been shown to work in opposition without reaching such a low saturation angle by the STAR Lab student Christian Haughwout. Recent preliminary tests performed in the lab have shown that the round wires do also buckle when being actuated against each other, but due to their slightly higher torque, they are capable of reaching a higher angle before stagnation. Unfortunately,

the higher second moment of area presents an important issue: the solar panel is not capable of being fully stowed without over-straining and damaging the SMA wire. The buckling issue is currently being studied and is an item for future work so we can understand the cause and how to avoid it.

Two paths are being pursued to solve the constraining issue of the hinge:

- Eliminating one constraint: The buckling straps should prevent the nonactive SMA from jumping out of its rail, but is currently preventing the SMA strip from stretching and/or moving. The idea is to change the shape and the tightness of these straps so they would allow the SMA to slide along its main axis, providing the extra accommodation the strips need. This design is currently being fabricated and is going to be tested soon as part of future work;

- Rethinking the hinge position: The buckling happens basically because the nonactive strip is being forced in a shape that is the extreme opposite of its trained shape. The idea here is to avoid the need of bending the SMA backwards by installing the hinge on the wall of the CubeSat instead of on the top of the satellite. This plane change would allow one SMA to be trained to a flat position and the other SMA to be trained to 180°, making the SMA's range from bent to not bent, instead of from bent in one direction to bent in the opposite direction, avoiding this middle singularity point. This idea is also being currently fabricated and is going to be tested soon as part of future work.

4.3 Parabolic Flight Expectations

The results we plan to retrieve from the parabolic flight will characterize the performance of the FLAPS mechanism for future use in small satellites, as the zero gravity situation is a lot more similar to the real environment that satellites are exposed to.

We are going to measure angle, response time and temperature, and power without without gravity. We expect the hinge to work better with less gravity, as the weight of the solar panel (or any actuated surface) applies an undesired and unnecessary

bending moment on the hinge, increasing the force threshold that the SMA needs to overcome to actuate the mechanism. We expect the actuation angle to be larger (especially after the buckling issue is solved) and the actuation speed to be faster.

Chapter 5

Conclusions

5.1 Summary of the Findings and Results

Initial lab tests show that the hinge prototype and controller can actuate successfully to angles between 0° (stowed position) up to approximately 18° (deployed position), with future work to improve actuation to more than 90°. Note that the annealed SMA is able to reach higher angles when it is tested outside the hinge, showing the the annealing and shape memory affect are not the issues.

In the initial design, the hinge is driven by two opposing SMA strips. The active strip provides approximately 1.4 lbf of bending force, while the opposing strip offers approximately 0.23 lbf of resisting force, resulting in a positive net force capable of deploying the hinge.

The system appears to have a range of linear behavior, i. e., the actuation angle is proportional to the input power up to approximately 0.15 W. The transfer function is of second order and the tuned PID gains were capable of achieving a smaller than 2° actuation error.

With hinge limitation, the actuation angle of the hinge ranged from 0 to almost 20° depending on the provided power and the thickness of the SMA strip. The saturation angle was the limiting factor in the hinging range.

Further design iterations have the goal of improving the actuation capabilities and range of operations, mainly due to the overconstraint encountered in the current

hinge design.

5.1.1 Reached Goals

The Folded Lightweight Actuation Precision System (FLAPS) project main goal was to develop a mechanical actuator that is small and lightweight, repeatable and precise. The hinge-SMA system is:

- Small: the outside dimensions of each hinge part is 50 mm x 40 mm x 12 mm;
- Lightweight: the mass of the complete hinge assembly is only 35 g;
- Repeatable: the angles reached by the actuator can be achieved many times in a row with minimal error;
- Precise: the set point was achieved within a 2° error and we will try to improve this too.

Even though the system does not fully actuate to more than 90° and is yet to be tested in the low gravity environment, the progress towards achieving all goals is significant, with plans for future work to meet all requirements.

5.2 Next Steps

The next steps for focus are addressing the current issues that are already being worked on:

- The buckling issue: for the hinge to be able to fully actuate, the buckling needs to be addressed. The current ideas are changing the flat strips for round wires, eliminating the overconstraints of the hinge, and changing the position of the SMA actuators within the hinge;
- Refining the control scheme: the accuracy of the transfer function could be improved if more SMA samples of different thicknesses were tested multiple

times. The gains of the PID controller can also be improved if more testing and analysis is put into it, aiming to balance speed and accuracy;

- Perform the zero gravity tests: the results from the zero gravity flight will help understand the influence of the surface weight on the actuation performance, allowing us to refine the design of the hinge and the controllers;

- Consider running a preheat loop: as described in the approach and in the results section, there is a delay between when the power starts flowing through the SMA and when the actuation starts due to the time it takes to heat the SMA up. This delays decreases the precision of the transfer function. Adding a preheat loop that maintains the SMA on the edge of actuating would significantly decrease this delay and increase the model precision;

- Add an SMA electrical resistance monitoring sensor: it is not hard to poorly re-anneal the SMA strips to different positions if too much power is flown through it. On the other hand, the resistance of the SMA changes as its temperature increases, especially right before actuating. It would be interesting to monitor the SMA strip resistance to know when the hinge is indeed actuating and to avoid overheating the nitinol.

These action items are going to be addressed during the next months by the FLAPS team.

5.3 Recommendations for Future Work

Some improvements that should be addressed in the long term to provide a better actuation performance include:

- Perform lifetime and destructive testing to determine the points of failure of the proposed design;

- Perform environmental testing to evaluate the actuator performance under vacuum, thermal variation, and vibration;

- Perform thermal modeling of on-orbit environments to ensure the activation temperature of the nitinol would not be unintentionally reached;
- Look into different SMA materials that have higher transition temperatures;
- Study the range of motions necessary to achieve the most common on-orbit deployments and actuations;
- Develop an interface for the electrical, mechanical, thermal, and software design with a host spacecraft.

Bibliography

[1] TiNi Aerospace. Frangibolt. https://tiniaerospace.com/products/space-frangibolt/, May 04, 2019.

[2] Mario Melendrez Contreras. Design, analysis, and control of a nitinol shape memory alloy rotary actuator for spacecraft deployable structures. Bachelor thesis, Massachusetts Institute of Technology, Mechanical Engineering Department, June 2019.

[3] Sierra Neva Corporation. Space technologies - product catalog. Space Systems, Louisville, Colorado, 2015.

[4] Zero Gravity Corporation. Zero gravity research. Program Package 2, Arlington, VA, USA, January 2019.

[5] Marcia Dunn. Big test coming up for tiny satellites trailing mars lander. *https://phys.org/news/2018-11-big-tiny-satellites-trailing-mars.html*, March 17, 2019.

[6] Peter Fortescue, Graham Swinerd, and John Stark. *Spacecraft Systems Engineering*, chapter 15, pages 495–526. John Wiley & Sons, Ltd, fourth edition, 2011.

[7] Northrop Grumman. Products and capabilities. *http://www.northropgrumman.com/BusinessVentures/AstroAerospace/Products/Pages/default.aspx*, April 06, 2019.

[8] Allen Guzik and Othmane Benafan. Design and development of cubesat solar array deployment mechanisms using shape memory alloys. In *Proc. 44th Aerospace Mechanisms Symposium*, pages 375–388, NASA Glenn Research Center, May 2018.

[9] Darren Hartl and Dimitris C. Lagoudas. Aerospace applications of shape memory alloys. In *Proc. Institution of Mechanical Engineers - Part G: Journal of Aerospace Engineering*, USA, April 2007.

[10] Jaronie Mohd Jani, Martin Leary, Aleksandar Subic, and Mark A. Gibson. A review of shape memory alloy research, applications and opportunities. *Materials and Design*, (56):1078–1113, December 2013.

[11] Maxim O. Khatsenko. A rotary shape memory alloy actuator for cubesat deployable structures. Master's thesis, Massachusetts Institute of Technology, Mechanical Engineering Department, June 2017.

[12] Xin Lan, Jinsong Leng, and Shanyi Du. Design of a deployable antenna actuated by shape memory alloy hinge. *Materials Science Forum*, 546-549:1567–1570, May 2007.

[13] Leonardo Lecce and Antonio Concilio. *Shape Memory Alloy Engineering: for Aerospace, Structural and Biomedical Applications.* Elsevier, first edition, 2015.

[14] Y. Lien, G. Thoen, O. Grasvik, J. Bru, K. Paulsen, L. O. Lierstuen, B. Chamayou, D. Pinard, and I. McKenzie. Opto-pyrotechnics for space applications. In *Proc. International Conference on Space Optics*, Greece, October 2010.

[15] Matthew Long, Allen Lorenz, Greg Rodgers, Eric Tapio, Glenn Tran, Keoki Jackson, and Robert Twiggs. A cubesat derived design for a unique academic research mission in earthquake signature detection. In *Proc. 16th USU Conference in Small Satellites*, Utah, USA, August 2002.

[16] A. P. Markopoulos, I. S. Pressas, and D. E. Manolakos. A review on the machining of nickel-titanium shape memory alloys. *Rev. Adv. Mater. Sci.*, 42:28–35, March 2015.

[17] NASA. Nuclear spectroscopic telescope array, or nustar. Press Kit, JPL, Pasadena, California, June 2012.

[18] NASA. Mars reconnaissance orbiter. *https://nssdc.gsfc.nasa.gov/nmc/spacecraft/display.action?id=2005-029A*, March 17, 2019.

[19] Jamie K. Paik and Robert J. Wood. A bidirectional shape memory alloy folding actuator. *Smart Mater. Struct.*, 21, May 2012.

[20] Jenny Rumburg. Nasa's science mission directorate cubesat initiative. *https://www.nasa.gov/content/goddard/nasas-science-mission-directorate-cubesat-initiative*, March 17, 2019.

[21] Oxford Space Systems. Technology. https://oxford.space/#1553262389480-619f91ae-3875, May 06, 2019.